**MAJOR REPORT**

# Particle physics using reactor antineutrinos

IOP Publishing Journal of Physics G: Nuclear and Particle Physics
J. Phys. G: Nucl. Part. Phys. **51** (2024) 080501 (50pp) https://doi.org/10.1088/1361-6471/ad3a84

**Major Report**

# Particle physics using reactor antineutrinos

**O A Akindele[1], N S Bowden[1,*], C Roca[1], J Xu[1], X Zhang[1], J M Berryman[2,3], R Carr[4], A J Conant[5], G Fernandez-Moroni[6], P Huber[7], J M Link[7], T J Langford[8], B R Littlejohn[9,*], J P Ochoa-Ricoux[10,*], L Strigari[11], S Schoppmann[2,12,14] and C Zhang[13]**

[1] Lawrence Livermore National Laboratory, Livermore, CA, United States of America
[2] Department of Physics, University of California, Berkeley, CA 94720, United States of America
[3] Institute for Nuclear Theory, University of Washington, Seattle, WA 98195, United States of America
[4] Department of Physics, United States Naval Academy, Annapolis, MD, United States of America
[5] Oak Ridge National Laboratory, Oak Ridge, TN, United States of America
[6] Fermi National Accelerator Laboratory, PO Box 500, Batavia, IL 60510, United States of America
[7] Center for Neutrino Physics, Virginia Tech, Blacksburg, VA, United States of America
[8] Wright Laboratory and Department of Physics, Yale University, New Haven, CT 06511, United States of America
[9] Department of Physics, Illinois Institute of Technology, Chicago, IL, United States of America
[10] Department of Physics and Astronomy, University of California, Irvine, CA 92697, United States of America
[11] Texas A&M University, College Station, TX 77843, United States of America
[12] Lawrence Berkeley National Laboratory, Berkeley, CA 94720, United States of America
[13] Physics Department, Brookhaven National Laboratory, Upton, NY 11973, United States of America

E-mail: nbowden@llnl.gov, blittlej@iit.edu and jpochoa@uci.edu

Received 15 September 2023, revised 17 November 2023
Accepted for publication 4 April 2024
Published 26 June 2024


**Abstract**

Nuclear reactors are uniquely powerful, abundant, and flavor-pure sources of antineutrinos that have played a central role in the discovery of the neutrinos and in elucidation of their properties. This continues through a broad range of experiments investigating topics including Standard Model and short-baseline oscillations, beyond-the-Standard-Model physics searches, and reactor flux

[14] Current address: Detektorlabor, Exzellenzcluster PRISMA$^+$, Johannes Gutenberg-Universität Mainz, 55128 Mainz, Germany.
[*] Authors to whom any correspondence should be addressed.

 

and spectrum modelling. This Report will survey the state of the reactor antineutrino physics field and summarize the ways in which current and future reactor antineutrino experiments can play a critical role in advancing the field of particle physics in the next decade.

Keywords: neutrino, nuclear reactor, reactor neutrino, reactor antineutrino, particle physics, reactor core, antineutrino

## 1. Introduction

Nuclear reactors are a uniquely powerful, abundant, and flavor-pure source of MeV-scale antineutrinos. Electron-flavored antineutrinos ($\overline{\nu}_e$) are produced in reactors as the unstable, neutron-rich products of nuclear fission undergo beta decay reactions:

$$^{A}_{Z}B_N \rightarrow {}^{A}_{Z+1}C_{N-1} + e^- + \overline{\nu}_e. \quad (1)$$

While only a few percent of the the roughly 200 MeV of excess rest mass energy from one nuclear fission is ultimately expressed as $\overline{\nu}_e$ kinetic energy, this equates to a total release of $2 \times 10^{20}$ $\overline{\nu}_e$ per GW of thermal power generated. The energy spectrum of $\overline{\nu}_e$ emitted by an operating reactor core reflects the decay schemes of the decaying isotopes, whose endpoints roughly range from the sub-MeV to the 10 MeV scale, as well as the relative abundance of these isotopes in the nuclear fuel, which is driven primarily by the likelihood of their production (or yield) in the core's fission reactions (Way and Wigner 1948, Vogel *et al* 1981, Sonzogni *et al* 2015, Hayes and Vogel 2016).

The antineutrino emissions of dozens of nuclear reactors across three different continents have been observed with neutrino detectors. Locations of current and recent experiments are illustrated in figure 1. Most of these have been at commercial power reactors, which operate in the $\sim$GW$_{\text{th}}$ regime and burn fuel with a relatively low level of $^{235}$U enrichment (low enriched, or LEU). These reactors' neutrino emissions are produced by a mixture of fissionable isotopes, with the dominant isotopes $^{235}$U and $^{239}$Pu providing >80% of all fissions, and $^{238}$U and $^{241}$Pu each providing less than 10%. A number of experiments have also been performed at research reactors operating at substantially lower power, $\sim$10–100 MW$_{\text{th}}$. These cores have generally been smaller in spatial extent (<1 m dimensions) than commercial ones (>m dimensions), and have used fuel of substantially higher $^{235}$U enrichment (highly enriched, or HEU), leading to $\overline{\nu}_e$ emissions overwhelmingly dominated by $^{235}$U fission products. While other reactor types exist that contain substantially different fuel content than these two options, such as mixed oxide (Jaffke and Huber 2017, Bernstein *et al* 2018, Behera *et al* 2020) or natural uranium reactors (Carroll *et al* 2018), no measurements of these reactor types have been performed.

As different fission isotopes have differing yet overlapping fission product yields, HEU and LEU reactors modestly differ in the mean number and energy spectrum of neutrinos they release per fission. Considering the decay production mechanism in equation (1), predictions of HEU and LEU reactor $\overline{\nu}_e$ emissions can be composed by relying either on knowledge of the produced parent and daughter nuclei, referred to as the *summation* or *ab initio* approach (Vogel *et al* 1981, Mueller *et al* 2011, Fallot *et al* 2012, Sonzogni *et al* 2015, Estienne *et al* 2019), or on knowledge of the properties of the decay electron produced in concert with each $\overline{\nu}_e$, referred to as the *conversion* approach (Von Feilitzsch *et al* 1982, Schreckenbach *et al* 1985, Hahn *et al* 1989, Huber 2011). These prediction methods are described in further detail in section 7.

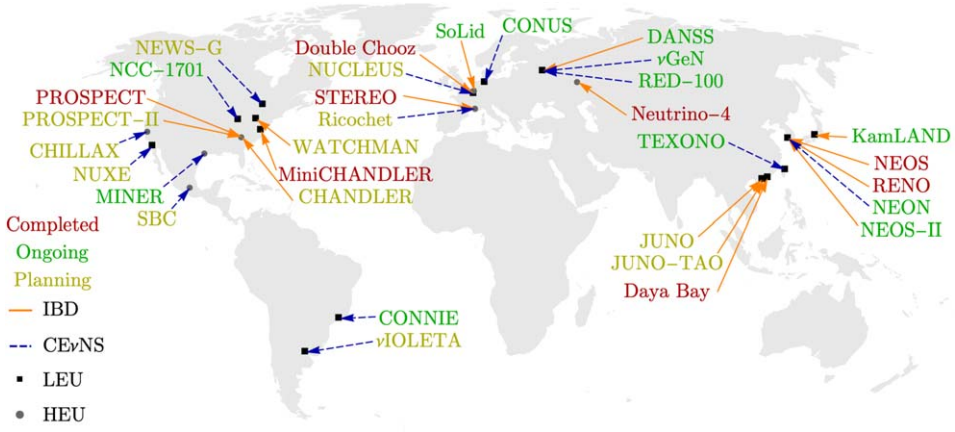


**Figure 1.** Map of planned, current, and completed reactor antineutrino experiments. Text color indicates experimental status, while arrow color indicates the interaction channel used by the experiment. Only completed experiments taking data after 2010 are included. Further description of these experiments are given in tables 3 and 4.

Reactor $\overline{\nu}_e$ can be detected via multiple detection channels, including inverse beta decay (IBD) on protons or other nuclei, neutral current inelastic nuclear scattering, neutrino-electron elastic scattering, and coherent elastic neutrino-nucleus scattering (Qian and Peng 2019). The proton IBD interaction, $p + \overline{\nu}_e \rightarrow n + e^+$, represents the vast majority of all observed interactions to date. The presence of two final-state particles that can be individually and coincidentally detected in organic scintillator detectors is advantageous in achieving excellent background reduction; this channel also facilitates high-fidelity determination of $\overline{\nu}_e$ energies via reconstruction of $e^+$ energies. Detectors with some combination of very low background contamination, very low energy detection thresholds, and specialized materials are required for detection of reactor $\overline{\nu}_e$ using other detection channels. As an example, detection via coherent neutrino-nucleus scattering requires cryogenic detectors using semiconductors or bolometric crystals as targets, with energy detection thresholds well below 1 $keV_{nr}$ (nuclear-recoil). Figure 1 also indicates the exploited interaction channel in recent and future reactor $\overline{\nu}_e$ experiments.

Past reactor antineutrino experiments have been critically important in the elucidation of the contemporary view of the Standard Model (SM) of particle physics. Proton IBD-based reactor measurements were the first to verify the existence of neutrinos (Reines and Cowan 1959), and have yielded world-leading or competitive precision on three of the six SM neutrino mixing parameters (Eguchi *et al* 2003, Araki *et al* 2005, Abe *et al* 2012b, Ahn *et al* 2012, An *et al* 2012, An *et al* 2014). Deuteron IBD-based reactor measurements provided early validations of weak interaction theory (Pasierb *et al* 1979). Reactor $\overline{\nu}_e$-electron scattering measurements have enabled measurement of the Weinberg mixing angle and competitive limits on measurements of the magnetic moment of the neutrino (Reines *et al* 1976, Deniz *et al* 2010). Reactor experiments have also enabled world-leading probes of new beyond-the-Standard-Model (BSM) physics. Short-baseline proton IBD experiments have been used to set new limits on active-sterile neutrino mixing in the eV-scale range and below (Declais *et al* 1995, An *et al* 2016d, Ko *et al* 2017, Alekseev *et al* 2018, Almazán *et al* 2020b, Andriamirado *et al* 2021a, Serebrov *et al* 2021). Efforts to measure reactor-based coherent neutrino scattering, while so far unsuccessful in detecting a statistically significant quantity of neutrino

interactions, have nonetheless established world-leading limits on some prospective hidden sector couplings to neutrinos (Aguilar-Arevalo *et al* 2020, Colaresi *et al* 2021). All of these measurements have been performed with fairly imprecise knowledge regarding the true underlying flux and spectrum of reactor $\overline{\nu}_e$ emissions.

In the coming decade, reactor-based neutrino measurements will continue to provide crucial new insights into the nature of the SM and beyond. New reactor-based oscillation experiments can continue extending the boundaries of our understanding of key SM mixing parameters (An *et al* 2016a, Littlejohn *et al* 2020, Ochoa-Ricoux *et al* 2020), while also pushing active-sterile mixing parameter space coverage in the electron flavor sector close to the few-percent level over a wide range of mass splittings from $\Delta m^2_{13}$ to the 10 s of $\mathrm{eV}^2$ scale (Abusleme *et al* 2020, Cao *et al* 2020, PROSPECT Collaboration 2020a, 2020b, Andriamirado *et al* 2022). Future high-statistics $\overline{\nu}_e$ measurements at differing reactor types can greatly improve our understanding of the absolute flux and spectrum of reactor $\overline{\nu}_e$ produced by all reactor core types, both above and below the 1.8 MeV IBD interaction threshold (Conant and Surukuchi 2020). In addition to improving the achievable precision of some reactor-based BSM measurements, such as those performed by CEvNS experiments, these improvements are clearly synergistic with facets of the applied reactor physics, nuclear safeguards, and nuclear data communities (Fallot *et al* 2019, Akindele and Zhang 2020, PROSPECT Collaboration 2020c, Akindele *et al* 2021, Romano *et al* 2022).

This Report is organized as follows: sections 2 and 3 will begin by summarizing the role that reactor antineutrinos can play in modern particle physics and potential synergies with other experimental neutrino sources and fields of study. Sections 4 and 5 highlight the potential improvements in understanding of SM oscillations and current short-baseline neutrino anomalies that can be achieved using reactor antineutrinos. Section 6 discusses how future reactor measurements can improve knowledge of other SM neutrino properties and possible hidden-sector couplings. Section 7 overviews potential advancements in global understanding of $\overline{\nu}_e$ emissions from various reactor types and the ability to accurately model these emissions. Finally, section 8 will focus on detector technology developments relevant to reactor $\overline{\nu}_e$ experiments.

## 2. Synergies between reactor antineutrinos and neutrino physics

Reactor $\overline{\nu}_e$ data plays a variety of essential roles in performing future SM and BSM oscillation measurements vital to the US neutrino community. Their power and complimentary position in the global landscape is well illustrated in figures 2 and 3. As they sample lower neutrino energies than most other efforts (figure 2), reactor experiments can feasibly access all $\Delta m^2$ ranges of interest in current oscillation studies with a single source type. They also sample a pure flux of electron-flavor neutrinos (figure 3), enabling particularly clean tests of specific mixing parameters. Since lower energies in reactor experiments are also accompanied by shorter baselines, reactor-based oscillation tests are also less influenced by some commonly-studied neutrino sector BSM effects, such as non-standard matter interactions or heavy-mediator couplings between neutrinos and hidden sectors.

In the context of the today's US neutrino program, one of reactor experiments' most prominent roles is in testing the origin of anomalies observed by short-baseline neutrino experiments. This topic addresses two of the five Science Drivers identified in the 2014 P5 report (Ritz *et al* 2014). Many of these persistent anomalies rest in the electron flavor realm, where reactor experiments, in particular, excel. For example, the BEST experiment recently confirmed the robustness of the so-called 'Gallium Anomaly' by detecting a $\sim$20% deficit in

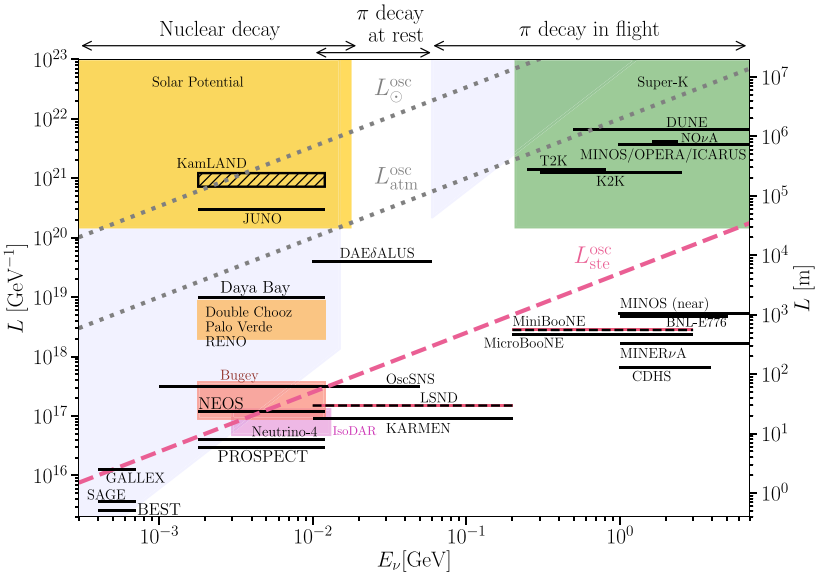


**Figure 2.** Overview of experimental source-detector baselines (L) and neutrino energies (E) sampled by neutrino experiments worldwide. Figure taken from Argüelles *et al* (2023).

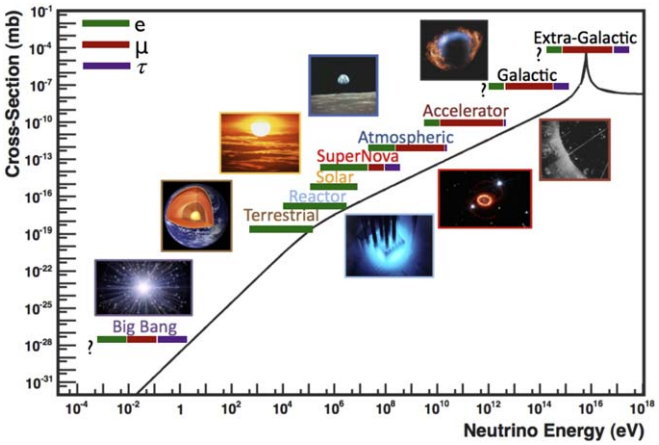


**Figure 3.** Approximate flavor composition of commonly discussed neutrino sources. Figure adapted from Formaggio and Zeller (2012). Reactor experiments are notable in their use of lower energy neutrinos, their access to very short baselines, and their extreme electron flavor purity.

observed interactions of sub-MeV $\nu_e$ generated by an intense radioactive source (Barinov *et al* 2022a). Even MicroBooNE, which primarily samples $\nu_\mu$ from Fermilab's BNB beamline, has attracted attention with weak hints of a deficit of $\nu_e$ interactions (Abratenko *et al* 2022), prompting further theoretical examination of sterile-mediated electron-flavor disappearance (Argüelles *et al* 2022, Denton 2022). This recent result contrasts with long-standing MiniBooNE results showing an excess of $\nu_e$-like events in the same beamline (Aguilar-Arevalo *et al* 2021).

Future aspects of the US neutrino program, such as Fermilab SBN (Antonello *et al* 2015), will certainly fight in the following decade to elucidate the causes of these and other anomalies. However, when viewed in the canonical BSM framework of oscillations between three active neutrino states and one additional sterile state (3 + 1), it seems likely that conclusively demonstrating the consonance or dissonance of these varied datasets will be a challenging task. Datasets that test, with maximal clarity, the 3 + 1 oscillation interpretation in specific channels and suggested phase space regions are a particularly important ingredient in this effort. Short-baseline reactor neutrino experiments, with their well-defined flavor profile, straightforward energy reconstruction, and purely relative analysis methods, offer an ideal experimental arrangement for targeted, clear tests. For these reasons, reactor experiments are a crucial piece of a diverse future global effort capable of elucidating whether or not a 3 + 1 model is an acceptable solution to the various short-baseline anomalies.

It is also possible that the observed short-baseline anomalies are instead explained by a hidden sector physics scenario more complex than the canonical 3 + 1 model, such as one with multiple sterile neutrinos (3 + N) (Kopp *et al* 2013), sterile neutrino decay (de Gouvêa *et al* 2020, Dentler *et al* 2020), non-standard interactions (NSI) (Bhupal Dev *et al* 2019), hidden sector couplings (Batell *et al* 2009), or some combination of effects (Moss *et al* 2018). If this is the case, data from diverse channels, energies, and sources will be even more crucial for disentangling the different contributing effects, as each effect may or may not manifest itself differently in specific experimental regimes. In the stable of global measurements, short-baseline reactor oscillation measurements are unique in their capability to very purely probe sterile oscillation effects. As mentioned above, this is due to the lower energies involved in interactions and decays in the reactor, which prohibits production and decay of heavier hidden-sector particles, and their very short baselines, which minimize the impact of NSI.

Short-baseline reactor experiment results also have particular relevance to upcoming measurements of SM neutrino properties. Theoretical studies have pointed to specific regions of 3 + 1 phase space that could complicate interpretation of DUNE and other future US long-baseline neutrino measurements (de Gouvêa *et al* 2015, Klop and Palazzo 2015). For example, a sterile sector with specific combinations of non-zero active and sterile CP violating phases could mimic CP-conserved signatures in DUNE (Gandhi *et al* 2015). Parameter degeneracies can be avoided for DUNE if separate measurements are used to constrain the level of active-sterile mixing; scenarios like the one above can be avoided if limits on $\theta_{14}$ and $\theta_{24}$ can be improved to approximately the 5° ($\sin^2 2\theta = 0.03$) level (Dutta *et al* 2016). $\theta_{14}$ limits meeting this stringent requirement are only accessible with intense electron-flavor sources, such as reactors and tritium decay facilities like KATRIN and Project-8 (Aker *et al* 2021). Thus, reactor $\overline{\nu}_e$ experiments play a synergistic role in enabling clear interpretations of the next generation experiment, DUNE, and its physics centerpiece, measurement of leptonic CP-violation.

Medium- and long-baseline reactor oscillation measurements are also crucial in extending neutrino oscillation measurements. It should first be emphasized that reactor-based measurements of a large $\theta_{13}$ value paved the way for DUNE by demonstrating that CP-violation measurements are feasible with conventional neutrino beams. In the near future, Daya Bay's still-improving limits on $\theta_{13}$ remain essential in current accelerator-based probes of CP-violation with T2K and NOvA (Acero *et al* 2022, Abe *et al* 2021), and later, when included in DUNE fits, they will modestly enhance DUNE's oscillation parameter measurement precision (Bass *et al* 2015). Approached from a different perspective, comparisons of Daya Bay's and DUNE's independently-measured $\theta_{13}$ values can be directly compared to yield tests of unitary in the PMNS mixing matrix (Qian *et al* 2013, Ellis *et al* 2020). In the solar sector, JUNO, along with DUNE, are the primary pieces in a future program for sharpening our view of

tensions in solar- and reactor-derived measurements of $\Delta m^2_{21}$ (Capozzi *et al* 2019); if such a discrepancy persists in these higher-precision experiments, it could provide the first clear evidence for non-standard neutrino interactions (Bhupal Dev *et al* 2019). Last but not least, JUNO will measure the mass hierarchy independently of other experiments (Abusleme *et al* 2022a), providing unique information on a parameter that is extremely important across many branches of neutrino physics, including neutrinoless double beta decay and neutrino mass experiments, as well as DUNE's long-baseline oscillation (Abi *et al* 2020a, Abud Abed *et al* 2022) and supernova neutrino burst (Abi *et al* 2021) physics programs.

## 3. Synergies of reactor antineutrinos beyond neutrino physics

Beyond the high energy physics topics mentioned in the previous section, reactor $\overline{\nu}_e$ measurements can contribute to other fields of scientific inquiry. As described in section 7, the $\overline{\nu}_e$ emissions from a reactor provide a probe of the nuclear fission process that is complementary to other techniques that measure more readily accessible particles like fission fragments, gamma-rays and neutrons. Specifically, the reactor $\overline{\nu}_e$ energy spectrum encodes information about fission product yields and the energy spectrum of beta-decays of those fission daughters. Included in the total $\overline{\nu}_e$ spectrum are contributions from short-lived, high Q-value isotopes, some of which have received limited experimental investigation. High statistics and high precision $\overline{\nu}_e$ spectrum measurements therefore have the potential to test the nuclear data evaluations that underlie many areas of nuclear physics, nuclear energy, and nuclear security. Nuclear data needs and benefits that can be addressed with reactor $\overline{\nu}_e$ have been described in recent workshops and reports (Fallot *et al* 2019, Romano *et al* 2022).

Advances in scientific knowledge regarding neutrino production in nuclear reactors and characterizing such nuclear systems themselves also underlie another significant societal benefit of reactor $\overline{\nu}_e$ studies. As described in (Bernstein *et al* 2020), the $\overline{\nu}_e$ emitted by operating nuclear reactors and spent nuclear fuel may be useful for cooperative nonproliferation applications such as monitoring fissile material production in reactors, exclusion of undeclared reactors, and monitoring of spent fuel and reprocessing facilities.

A recent study focused on the potential utility of $\overline{\nu}_e$ for nuclear energy and nuclear security applications elucidates some of the relevant characteristics of these particles and potential use cases for them (Akindele *et al* 2021). The highly penetrating nature of neutrinos poses detection and implementation challenges in the context of monitoring applications, but also holds promise as a non-intrusive technique that does not require direct access to complex and/or sensitive facilities. Considering user need and constraints, forthcoming advanced reactor types for which nuclear safeguards techniques are still be developed and nuclear security deals between nations were found to be promising use cases for $\overline{\nu}_e$ monitoring measurements.

Of course, potential applications of $\overline{\nu}_e$ depend heavily upon the detection tools and techniques developed by neutrino physics experiments. All application oriented demonstrations of reactor $\overline{\nu}_e$ have been enabled by the multi-decade succession of reactor $\overline{\nu}_e$ scientific experiments that have preceded them (Bernstein *et al* 2020). Recent advances like aboveground $\overline{\nu}_e$ detection without substantial overburden (Ashenfelter *et al* 2018, Haghighat *et al* 2020) have greatly broadened the range of applications that can be considered. Since neutron identification is central to detection of the IBD interactions, materials and techniques developed for reactor $\overline{\nu}_e$ also have significant potential for neutron detection in support a wide range of nuclear security applications (Runkle *et al* 2010).

Beyond the scope of neutrino oscillation physics and potential applications, reactor $\overline{\nu}_e$ experiments continue to develop technologies well-suited for other areas in neutrino and particle physics. For example, technology being developed to enable detection of low-energy signals from coherent neutral current nuclear scattering of reactor $\overline{\nu}_e$ addresses similar challenges to those needed to seek dark matter interactions with electrons and nuclei (Agnolet *et al* 2017, Billard *et al* 2017, Aguilar-Arevalo *et al* 2019). Doped aqueous, plastic, or opaque scintillator technology used for reactor IBD detection may offer value in other sectors of the US neutrino physics program, such as in neutrinoless double beta decay experiments (Albanese *et al* 2021, Cabrera *et al* 2021), measurements of neutrino-induced neutron production (Back *et al* 2017), and future water-based DUNE far detector modules (Askins *et al* 2020). For these and other cases described in section 8, synergies clearly exist between the pursuit of reactor neutrino detection and other aspects particle physics.

## 4. Three-neutrino oscillation physics with reactors

In recent years, reactors have played a major role in the study of neutrino oscillations and helped establish the three-neutrino oscillation framework that still stands as the leading paradigm of this phenomenon (Vogel *et al* 2015, Zyla *et al* 2020). In this section, we review the theory, experiments, and prospects of three-neutrino oscillation physics with reactors.

### *4.1. Reactor antineutrino oscillations*

In the SM of particle physics, three neutrino flavors, $\nu_e$, $\nu_\mu$, and $\nu_\tau$, participate in the weak interaction. However, if neutrinos have a non-zero mass, the flavor composition of a neutrino beam could change as the neutrinos propagate in space. This phenomenon is called neutrino oscillations and is a quantum mechanical effect stemming from the fact that a neutrino with a definite flavor need not have a definite mass. In fact, a neutrino flavor eigenstate can be viewed as a linear superposition of the neutrino mass eigenstates, $\nu_1$, $\nu_2$, and $\nu_3$:

$$\begin{pmatrix}\nu_e\\ \nu_\mu\\ \nu_\tau\end{pmatrix} = \begin{pmatrix}U_{e1} & U_{e2} & U_{e3}\\ U_{\mu1} & U_{\mu2} & U_{\mu3}\\ U_{\tau1} & U_{\tau2} & U_{\tau3}\end{pmatrix}\cdot\begin{pmatrix}\nu_1\\ \nu_2\\ \nu_3\end{pmatrix}. \tag{2}$$

The unitary $3\times3$ mixing matrix, $U$, is called the Pontecorvo–Maki–Nakagawa–Sakata (PMNS) matrix and can be parameterized by three mixing angles, $\theta_{12}$, $\theta_{13}$, $\theta_{23}$, and one CP-violation phase, $\delta_{\mathrm{CP}}$[15]:

$$U_{\mathrm{PMNS}} = \begin{pmatrix}1 & 0 & 0\\ 0 & c_{23} & s_{23}\\ 0 & -s_{23} & c_{23}\end{pmatrix}\begin{pmatrix}c_{13} & 0 & s_{13}e^{-i\delta_{\mathrm{CP}}}\\ 0 & 1 & 0\\ -s_{13}e^{i\delta_{\mathrm{CP}}} & 0 & c_{13}\end{pmatrix}\begin{pmatrix}c_{12} & s_{12} & 0\\ -s_{12} & c_{12} & 0\\ 0 & 0 & 1\end{pmatrix}, \tag{3}$$

where the notation $c_{ij}=\cos\theta_{ij}$, $s_{ij}=\sin\theta_{ij}$ is used.

As neutrinos travel a certain distance $L$ in vacuum, their mass eigenstates with energy $E$ develop a phase such that $\nu_i(L)=e^{-i\frac{m_i^2}{2E}L}\cdot\nu_i(0)$. Given the neutrino mixing formula in equation (2), the probability of a neutrino with flavor $l$ transforming to a different flavor $l'$ can be written as:

[15] There are two additional phases if neutrinos are Majorana particles, but they do not play a role in neutrino oscillation experiments.

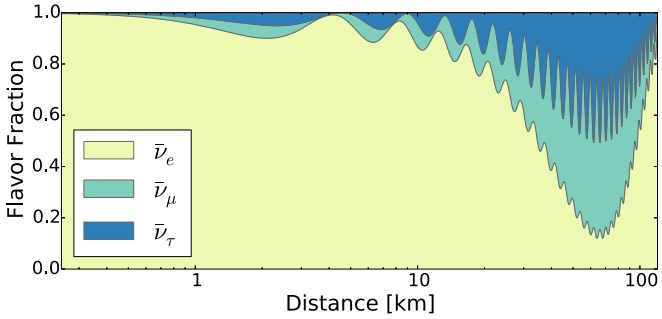


**Figure 4.** Expected flavor composition of the reactor antineutrino flux as a function of distance to a reactor core for neutrinos of 4 MeV energy. Figure taken from Vogel *et al* (2015). The light yellow region corresponds to the survival probability of $\bar{\nu}_e$ that reactor antineutrino experiments can measure by placing their detectors at different baselines.

$$\begin{aligned} P_{\nu_l \to \nu_{l'}} &= |<\nu_{l'}(L)|\nu_l(0)>|^2 \\ &= \left| \sum_j U_{lj} U^*_{l'j} \mathrm{e}^{-\mathrm{i}\frac{m_j^2}{2E}L} \right|^2 \\ &= \sum_j |U_{lj} U^*_{l'j}|^2 + \sum_j \sum_{k \neq j} U_{lj} U^*_{l'j} U^*_{lk} U_{l'k} \mathrm{e}^{\mathrm{i}\frac{\Delta m^2_{jk} L}{2E}}, \end{aligned} \tag{4}$$

where $\Delta m^2_{jk} = m^2_j - m^2_k$ are the mass-squared differences between mass eigenstates.

Since nuclear reactors produce only electron antineutrinos, $\bar{\nu}_e$, with an energy lower than the production threshold of a muon or a tau lepton, the experimental observation of neutrino oscillations is typically through the disappearance channel. Namely, the $\bar{\nu}_e$ neutrino flux is measured at some distance $L$ away from the reactor, and the survival probability $P_{\bar{\nu}_e \to \bar{\nu}_e}$ is calculated by comparing to the flux near the source. Given equation (4), this survival probability can be expressed as:

$$\begin{aligned} P_{\bar{\nu}_e \to \bar{\nu}_e} &= 1 - 4|U^2_{e1}||U^2_{e3}|\sin^2\Delta_{31} - 4|U^2_{e2}||U^2_{e3}|\sin^2\Delta_{32} - 4|U^2_{e1}||U^2_{e2}|\sin^2\Delta_{21} \\ &= 1 - \sin^2 2\theta_{13}(\cos^2\theta_{12}\sin^2\Delta_{31} + \sin^2\theta_{12}\sin^2\Delta_{32}) - \cos^4\theta_{13}\sin^2 2\theta_{12}\sin^2\Delta_{21}, \end{aligned} \tag{5}$$

where the notation $\Delta_{ij} = \frac{\Delta m^2_{ij} L}{4E}$ is used. From equation (5) we see that reactor antineutrino disappearance is a clean channel that is only dependent on $\theta_{12}$, $\theta_{13}$, $\Delta m^2_{21}$, $\Delta m^2_{31}$, and the neutrino mass ordering, making it ideal for precision measurements of these oscillation parameters. Figure 4 shows the survival probability as a function of the travel distance $L$ for a typical 4 MeV reactor $\bar{\nu}_e$. The large disappearance at ∼60 kilometers is driven by the solar-mixing mass scale $\Delta m^2_{21}$ and its corresponding large mixing angle $\theta_{12}$, while the smaller disappearance at ∼2 kilometers is caused by the atmospheric-mixing mass scale $\Delta m^2_{31} \sim \Delta m^2_{32}$ and the small mixing angle $\theta_{13}$. The two very different $\Delta m^2$ scales benefit designs of reactor antineutrino oscillation experiments, which can isolate the parameters of interest and improve the precision of their determination by placing detectors at strategic baselines.

### *4.2. Breakthroughs with reactor antineutrinos*

The first reactor antineutrino experiment that observed an evidence of neutrino oscillations is the KamLAND experiment (Eguchi *et al* 2003), built in the early 2000s in Japan. The KamLAND experiment was prompted by the 'Solar Neutrino Problem', which refers to the observation that the $\nu_e$ flux from the Sun is less than a half of the prediction from the Standard Solar Model (Davis *et al* 1968). The theory of neutrino oscillations provides an elegant solution to the solar neutrino problem, and can be tested on Earth using reactor antineutrinos assuming *CPT* invariance. The KamLAND experiment is located in the middle of Japan, surrounded by 55 Japanese reactor cores with a flux-weighted average baseline of ∼180 kilometers. As shown in figure 4, at this baseline, the KamLAND experiment is sensitive to the solar-mixing parameters $\Delta m^2_{21}$ and $\theta_{12}$, and benefits from a better understood neutrino source and simpler vacuum oscillation formula compared to solar neutrino experiments. The KamLAND detector uses one kiloton of liquid scintillator as the target volume, which is contained in a 13 meter-diameter transparent balloon surrounded by a mineral oil region containing 1879 photomultiplier tubes (PMTs). The results in 2008 observed a total of 1609 events with a 2.9 kton-year exposure, which was only about 60% of the predicted signal if there were no oscillations (Abe *et al* 2008). The calculated survival probability shows a clear oscillatory pattern as a function of $L/E_\nu$, decisive evidence of the existence of neutrino oscillations. The results were also highly consistent with solar neutrino experiments. When combined with the results from SNO (Ahmad *et al* 2002), they provided the most precise measurement of $\tan^2\theta_{12} = 0.47^{+0.06}_{-0.05}$ and $\Delta m^2_{21} = 7.59^{+0.21}_{-0.21} \times 10^{-5}$ eV$^2$ to date (Abe *et al* 2008).

The first generation of reactor $\theta_{13}$ experiments, CHOOZ (Apollonio *et al* 1999) and Palo Verde (Boehm *et al* 2001), did not observe $\bar{\nu}_e$ disappearance from reactors and only an upper limit of $\sin^2 2\theta_{13} < 0.10$ at 90% C.L. was set. In the 2000s, a new generation consisting of Daya Bay (An *et al* 2016b), Double Chooz (de Kerret *et al* 2022), and RENO (Ahn *et al* 2012), was initiated to measure the small mixing angle $\theta_{13}$.

Given the mass-scale $\Delta m^2_{31}$ suggested by the atmospheric neutrino experiments, the corresponding baseline for reactor antineutrino experiments is about 1–2 kilometers, as indicated in figure 4. All experiments adopted the strategy of performing a relative measurement between near and far functionally identical detectors to largely suppress the reactor and detector related systematic uncertainties. After some early indications in 2011 (Abe *et al* 2011, 2012, Adamson *et al* 2011), all three experiments reported clear evidence of $\bar{\nu}_e$ disappearance in 2012 with a few month's data taking (Abe *et al* 2012b, An *et al* 2012, Ahn *et al* 2012).

Among these experiments, the Daya Bay experiment, being the most sensitive one, excluded $\theta_{13} = 0$ at $5.2\sigma$ with 55 days of data (An *et al* 2012). The Daya Bay experiment is located near the six reactors of the Daya Bay nuclear power plant in southern China, with a total reactor power of 17.4 GW$_{\rm th}$. Daya Bay uses eight identical antineutrino detectors (ADs), with two ADs at ∼360 m from the two Daya Bay reactor cores, two ADs at ∼500 m from the four Ling Ao reactor cores, and four ADs at a far site ∼1580 m away from the 6-reactor complex. Each AD contains 20-tons of gadolinium-loaded liquid scintillator as the target volume. Each AD's target is viewed by 192 8-inch PMTs that yield an energy resolution of $8.5\%/\sqrt{E\,(\mathrm{MeV})}$, allowing a precise measurement of the reactor antineutrino energy spectrum that enables the observation of a spectral distortion between far and near detectors as expected from neutrino oscillations. In 2018 results, Daya Bay reported detection of nearly 3.5 million reactor antineutrino events in the near detectors and 500 thousand events in the far detectors over 1958 d of data collection. The comparison of relative $\bar{\nu}_e$ event rates and energy

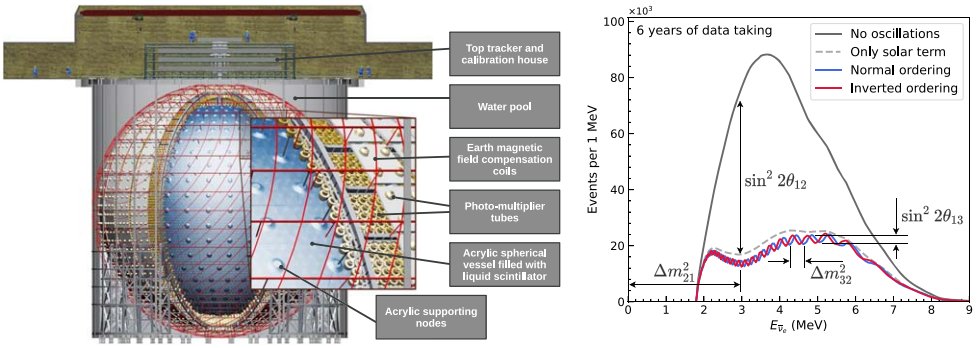


**Figure 5.** Left: schematic of the JUNO detector. An acrylic sphere containing 20 kilotons of liquid scintillator serving as the $\overline{\nu}_e$ detection target is surrounded by 20 inch and 3 inch PMTs. Right: JUNO IBD spectrum with and without neutrino oscillation effects. For illustration purposes, a detector with perfect energy resolution is assumed. The gray dashed curve shows the oscillated spectrum when only the term in the disappearance probability that is modulated by $\sin^2 2\theta_{12}$ is included, whereas the blue and red curves show it when the full oscillation probability in vacuum is used assuming the normal and inverted mass orderings, respectively. Some features driven by the $\sin^2 2\theta_{12}$, $\sin^2 2\theta_{13}$, $\Delta m^2_{31}$ and $\Delta m^2_{21}$ oscillation parameters are shown pictorially. Figures obtained from Abusleme *et al* (2022b).

spectra among detectors is consistent with the three-neutrino oscillation formula as introduced in equation (5) and yields $\sin^2\theta_{13} = 0.0856 \pm 0.0029$ and $\Delta m^2_{32} = 2.471^{+0.068}_{-0.070} \times 10^{-3}$ eV$^2$ assuming the normal mass ordering, and $\Delta m^2_{32} = -(2.575^{+0.068}_{-0.070}) \times 10^{-3}$ eV$^2$ assuming the inverted mass ordering (Adey *et al* 1958). The remarkable precision makes $\theta_{13}$ the most precisely measured angle among the three neutrino mixing angles in the PMNS matrix, despite being the last known mixing angle to be non-zero. The full data set of Daya Bay from 2012–2020, with over 6 million events, is the largest library of reactor antineutrino events collected in history, and is expected to further improve the precision of $\sin^2\theta_{13}$ and $\Delta m^2_{32}$ to better than 2.5% and 2%, respectively. Thanks to the consistent results reported by Double Chooz (Abrahão *et al* 2021) and RENO (Bak *et al* 2018), reactor experiments are providing robust and precise constraints to other experiments, including those searching for leptonic CP violation (Abe *et al* 2018, Abi *et al* 2020a, Abe *et al* 2021, Acero *et al* 2022).

### *4.3. Outlook: the JUNO experiment*

Beyond completion of these $\theta_{13}$ experiments, reactor antineutrino experiments continue to be at the forefront of neutrino oscillation physics. The Jiangmen Underground Neutrino Observatory (JUNO) is currently under construction in southern China and is expected to come online in 2023 (Abusleme *et al* 2022a). JUNO will be located at a baseline of ∼52.5 km from six 2.9 $GW_{th}$ nuclear reactor cores in the Yangjiang Nuclear Power Plant (NPP) and two 4.6 $GW_{th}$ cores in the Taishan NPP. As shown in figure 5, JUNO's central detector (CD) will consist of 20 kilotons of liquid scintillator contained in an acrylic sphere immersed in water and surrounded by 1761 220 inch and 256 003 inch PMTs providing more than 75% optical coverage. This central region will be supported by an external water Cherenkov veto detector, and a detector-top cosmic veto tracker and calibration house.

JUNO will see an unparalleled amount of light for a detector of this type, amounting to over 1300 photoelectrons per MeV. This, in combination with a comprehensive calibration

program that includes the 3 inch PMT system as a handle to assess any instrumental non-linearities in the 20 inch PMT system (Abusleme *et al* 2021), will result in an energy resolution of 3% at 1 MeV. The unprecedented detector size and energy resolution will allow to simultaneously observe the effects of both the solar and atmospheric oscillations for the first time. As illustrated on the right panel of figure 5, the former produces a 'slow' oscillation modulated by $\sin^2 2\theta_{12}$ with frequency $\Delta m^2_{21}$, while the latter causes a 'fast' oscillation modulated by $\sin^2 2\theta_{13}$ with frequency $\Delta m^2_{32}$. As also illustrated in figure 5, the oscillated spectrum changes slightly depending on the neutrino mass ordering, providing sensitivity to this parameter. This difference is caused by the interference effects that occur between the $\Delta m^2_{31}$ and $\Delta m^2_{32}$ terms in the oscillation probability of equation (5), which depend on the sign of $\Delta m^2_{31}$. Knowledge of the unoscillated reactor antineutrino spectrum is important for JUNO's physics goals, so the collaboration will deploy a satellite detector at a baseline of $\sim$30 m from one of the Taishan 4.6 $GW_{th}$ cores called the Taishan Antineutrino Observatory (JUNO-TAO) (Abusleme *et al* 2020). JUNO-TAO will be a 1 ton fiducial sphere of liquid scintillator loaded with gadolinium surrounded by silicon photomultipliers providing about 94% of coverage. It will be able to measure the unoscillated reactor antineutrino spectrum with an unprecedented energy resolution $\lesssim$2% at 1 MeV, thus eliminating any model dependencies in JUNO's oscillation measurements.

The conventional method to estimate JUNO's median sensitivity to the mass ordering is fitting the oscillated spectrum under the normal and inverted ordering scenarios and considering the difference in the minimum $\chi^2$ values. Using the configuration of An *et al* (2016a), a value of $\Delta\chi^2 = 10$ with 6 years of data taking is obtained, which corresponds to a sensitivity of about $3\sigma$. This configuration assumes ten nuclear reactors rather than the eight that will actually be built, but also uses lower estimates of the IBD detection efficiency and the PMT detection efficiency, among others. A reassessment of the sensitivity is underway but no significant changes are expected (Abusleme *et al* 2022a).

JUNO's approach to measuring the mass ordering is orthogonal to the one to be carried out by next-generation experiments relying on atmospheric (Adrian-Martinez *et al* 2016, Aartsen *et al* 2017) and accelerator (Abe *et al* 2018, Abi *et al* 2020) neutrinos. The latter use neutrinos in the $\sim$GeV energy scale traversing distances of hundreds or thousands of km, while JUNO's neutrinos will be in the $\sim$MeV scale and will only travel for 52.5 km. Likewise, the detection technology and the backgrounds will be completely distinct. Very importantly, JUNO's measurement is completely independent of the $\theta_{23}$ mixing angle and the $\delta_{CP}$ phase. Finally, JUNO's signal arises entirely from vacuum oscillations, whereas all other experiments rely on matter effects. For all these reasons, JUNO's measurement will greatly strengthen the community's confidence in the determination of this critical parameter.

JUNO's measurement is also complementary to that of other experiments in that it will provide synergistic information beyond the pure statistical addition of results. A combined analysis of JUNO's data with those of ongoing or near term atmospheric (Aartsen *et al* 2020, Chau *et al* 2021) or accelerator (Cabrera *et al* 2022) experiments could yield the first determination of the neutrino mass ordering to $\geqslant 5\sigma$ significance. This synergy occurs primarily because of a tension in the measured values of $\Delta m^2_{31}$ that arises when the wrong ordering is assumed. As a result, the first unambiguous determination of the neutrino mass ordering could be achieved this decade.

JUNO's large-statistics measurement of the oscillated spectrum with unprecedented energy resolution will also enable determination of the four oscillation parameters that drive the disappearance of reactor antineutrinos at its 52.5 km baseline: $\Delta m^2_{31}$, $\Delta m^2_{21}$, $\sin^2\theta_{12}$, and $\sin^2\theta_{13}$. The expected sensitivities to these parameters after 6 years of data-taking are shown

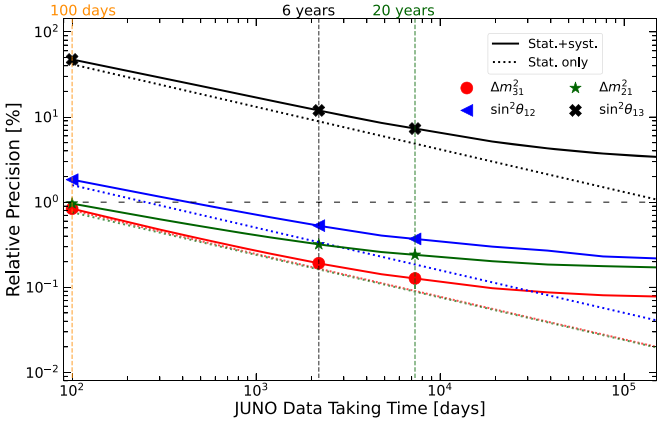


**Figure 6.** JUNO's relative precision on the oscillation parameters as a function of run time. The markers and vertical lines highlight run times of 100 d, 6 years, and 20 years. The horizontal gray dashed line represents a 1% relative precision. The green dotted and red dotted lines are indistinguishable from each other since the statistical-only precision is essentially identical for the $\Delta m^2_{31}$ and $\Delta m^2_{21}$ parameters. Figure taken from Abusleme *et al* (2022b).

**Table 1.** Expected precision of the oscillation parameters after 6 years of JUNO run time. All uncertainties are considered, and no external constraint is applied on $\sin^2\theta_{13}$. The precision with which these parameters are currently known is shown for comparison (Workman *et al* 2022). JUNO sensitivities obtained from Abusleme *et al* (2022b).

| | $\Delta m^2_{31}$ | $\Delta m^2_{21}$ | $\sin^2\theta_{12}$ | $\sin^2\theta_{13}$ |
|---|---|---|---|---|
| JUNO 6 years | 0.2% | 0.3% | 0.5% | 12.1% |
| PDG2020 | 1.4% | 2.4% | 4.2% | 3.2% |

in table 1. The expected relative precision is $\leqslant$0.5% for $\Delta m^2_{31}$, $\Delta m^2_{21}$ and $\sin^2\theta_{12}$, and the corresponding improvement over current knowledge for those parameters is around an order of magnitude. Figure 6 shows the expected precision as a function of running time for the four parameters. As can be seen there, the precision on $\Delta m^2_{21}$ and $\sin^2\theta_{12}$ will already be world-leading with only $\sim$100 d of data. Moreover, the precision of the four parameters will continue to improve appreciably even after 6 years of data-taking.

There is no confirmed experiment on the horizon that will be able to reach this precision on $\Delta m^2_{31}$, $\Delta m^2_{21}$ and $\sin^2\theta_{12}$, so these measurements are expected to be the best in the world for the foreseeable future. There are several ways in which they are expected to be an important input to the community:

(a) They will provide important constraints to present and future experiments.
(b) They will provide stringent inputs for neutrino masses and model building. For instance, the more precise knowledge of $\theta_{12}$ will play a prominent role, since this parameter is more sensitive to quantum corrections due to the fact that $\Delta m^2_{21} << |\Delta m^2_{31}|$ and because the non-zero value of $\theta_{13}$ can induce further corrections for $\theta_{12}$ (Harrison *et al* 2002, Xing 2002, He and Gang 2003).

(c) They will narrow down the parameter space of the neutrinoless double beta-decay effective mass $|m_{ee}|$. In inverted mass ordering scenarios where $m_3 < 0.05\,\text{eV}$, the minimal value of $|m_{ee}|$ is proportional to $\cos^2\theta_{12}$ (Lindner *et al* 2006). The better knowledge of $\theta_{12}$ will shrink the possible parameter space of $|m_{ee}|$ such that its minimum value can be increased by a factor of 2 (Ge and Rodejohann 2015). This will make a big difference to experiments (roughly a factor of 16 in the combined product of running time, detector mass, background level, and energy resolution for a background dominated experiment) and will thus have a strong impact on when and how a conclusive test of the inverted mass ordering region can be achieved (An *et al* 2016a).

(d) They will play a crucial role in model-independent tests of the three-neutrino oscillation framework, most notably unitarity tests of the PMNS matrix. For example, the combination of JUNO's results with those of short-baseline reactor experiments like Daya Bay and solar experiments like SNO will enable the first such direct test of $|U_{e1}|^2 + |U_{e2}|^2 + |U_{e3}|^2 = 1$ to the few percent level (Qian *et al* 2013, Fong *et al* 2017, Ellis *et al* 2020). Similarly, the combination of JUNO with muon (anti)neutrino disappearance measurements will enable tests of the mass sum rule $\Delta m^2_{13} + \Delta m^2_{21} + \Delta m^2_{32} = 0$, which is another important probe of physics beyond the SM such as the existence of sterile neutrinos.

In summary, reactor antineutrino experiments have played an essential role in unveiling the oscillatory behavior of the neutrino, from the first clear observation of the $L/E_\nu$ dependence of this phenomenon with terrestrial neutrinos, to the discovery of the non-zero value of $\theta_{13}$, among other breakthroughs. The precise determination of $\theta_{13}$ by reactor experiments already underpins the world's best knowledge on CP violation, and will continue to do so for the foreseeable future. Reactor antineutrinos will continue to have a prominent role in neutrino oscillation physics, with a measurement within this decade by JUNO of the neutrino mass ordering that is independent and complementary to what atmospheric and accelerator experiments can do. Likewise, by the end of this decade, the most precise knowledge of four out of the six parameters that drive neutrino oscillation will come from reactor antineutrino experiments, namely Daya Bay and JUNO, with three of these determined to 0.5% or better.

## 5. Non-standard flavor mixing searches at reactors

### *5.1. The reactor antineutrino anomaly*

In 2011, two independent reevaluations of the reactor antineutrino spectrum were published by Mueller *et al* (2011) and Huber (2011). Both concluded that the integrated antineutrino flux is ≈3% larger than previous calculations; we defer a discussion of the details of the flux model to section 7. Many of the authors of Mueller *et al* (2011) would then explicitly reanalyze reactor experiments dating back to the early 1980s in Mention *et al* (2011), finding that observed interaction rates were, on average, $(5.7 \pm 2.3)\%$ less than what the new 'Huber–Mueller' (HM) model predicted; this disagreement was named the *Reactor Antineutrino Anomaly (RAA)*. It is pertinent to consider whether modifications to three-neutrino oscillations might be the cause of the RAA.

The SM can be extended by introducing $N$ additional neutrino species. If these are light enough to participate in oscillations, then they must be uncharged under SM interactions, as the invisible decay width of the $Z$ boson is consistent with there being only three light neutrinos (Schael *et al* 2006). We refer to these as *sterile neutrinos* and denote them

$\{\nu_{s_1}, \nu_{s_2},\ldots,\nu_{s_N}\}$; these are accompanied by new mass eigenstates denoted $\{\nu_4, \nu_5, \ldots, \nu_{3+N}\}$. The mixing relationship given in equation (2) can be readily generalized to

$$\begin{pmatrix} \nu_e \\ \nu_\mu \\ \nu_\tau \\ \nu_{s_1} \\ \vdots \end{pmatrix} = \begin{pmatrix} U_{e1} & U_{e2} & U_{e3} & U_{e4} & \ldots \\ U_{\mu 1} & U_{\mu 2} & U_{\mu 3} & U_{\mu 4} & \ldots \\ U_{\tau 1} & U_{\tau 2} & U_{\tau 3} & U_{\tau 4} & \ldots \\ U_{s_1 1} & U_{s_1 2} & U_{s_1 3} & U_{s_1 4} & \ldots \\ \vdots & \vdots & \vdots & \vdots & \ddots \end{pmatrix} \cdot \begin{pmatrix} \nu_1 \\ \nu_2 \\ \nu_3 \\ \nu_4 \\ \vdots \end{pmatrix}; \tag{6}$$

the $3 \times 3$ PMNS matrix is replaced by a $(3 + N) \times (3 + N)$ analog. The sterile species, by construction, will not interact in a detector; one must infer their existence through their modifications to the oscillation probabilities of the active species. We focus on the case $N = 1$ for simplicity and replace $\nu_{s_1} \rightarrow \nu_s$. In this case, there are three unique mass-squared differences, $\{\Delta m^2_{21}, \Delta m^2_{31}, \Delta m^2_{41}\}$, and the $4 \times 4$ extended PMNS matrix may be written in terms of six mixing angles and three CP-odd phases. Here, we focus on the survival probability $P(\overline{\nu}_e \rightarrow \overline{\nu}_e) \equiv P_{\overline{e}\overline{e}}$ in the limit relevant to SBL reactor experiments. In the three-neutrino scenario, $P_{\overline{e}\overline{e}}$ does not deviate appreciably from unity for baselines $\lesssim \mathcal{O}(100)$ m at reactor energies. Therefore, any oscillations observed on $\mathcal{O}(10$–$100)$ m length scales would be attributable only to $\Delta m^2_{41}$. In the limit $\Delta_{21}, \Delta_{31} \approx 0$, we write

$$\begin{aligned} P_{\overline{e}\overline{e}} &\approx 1 - 4|U_{e4}|^2(1 - |U_{e4}|^2)\sin^2\Delta_{41} \\ &\equiv 1 - \sin^2 2\theta_{ee}\sin^2\Delta_{41}; \end{aligned} \tag{7}$$

where $\sin^2 2\theta_{ee}$ is the *effective mixing angle*. If $\sin^2 2\theta_{ee}$ is nonzero, then this can manifest as a deficit of $\overline{\nu}_e$ relative to prediction—precisely as indicated by the RAA.

In Mention *et al* (2011), rate experiments were explicitly analyzed with respect to the sterile neutrino hypothesis. It was found that the data prefer a sterile neutrino at the level $p \approx 3.5\%$; the preferred regions of parameter space were approximately $\sin^2 2\theta_{ee} \in [0.02, 0.20]$ and $\Delta m^2_{41} \gtrsim 0.40$ eV$^2$. When combined with anomalous $\nu_e$ disappearance results from the radioactive source experiments GALLEX (Hampel *et al* 1998, Kaether *et al* 2010) and SAGE (Abdurashitov *et al* 1999, 2006)—the so-called Gallium Anomaly (Acero *et al* 2008, Giunti and Laveder 2011b)—these become $p \approx 0.3\%$, $\sin^2 2\theta_{ee} \in [0.05, 0.22]$ and $\Delta m^2_{41} \gtrsim 1.45$ eV$^2$.

Since Mention *et al* (2011) first appeared, new measurements of the antineutrino rate at HEU reactors were performed at Nucifer (Boireau *et al* 2016) and STEREO (Almazán *et al* 2020a). Moreover, medium-baseline experiments have also become competitive in this endeavor. Double Chooz (de Kerret *et al* 2020), Daya Bay (An *et al* 2016c), and RENO (Choi *et al* 2016) all measured time-integrated antineutrino rates consistent with the RAA. These results supported the robustness of the suggested data-model flux discrepancy and hint for sterile neutrino oscillations. On the other hand, Daya Bay (An *et al* 2017c, Adey *et al* 2019b) and RENO (Bak *et al* 2019) have also exploited a particular feature of LEU reactors: they can track how the $\overline{\nu}_e$ detection rate evolves with the reactor fuel composition. They observe a dependence of the RAA size on fuel content, a clear indication of flux mis-modelling of some sort.

In parallel to these experimental developments, the HM $\overline{\nu}_e$ flux model has also been the subject of increased scrutiny. While modeling will be discussed in more depth in section 7, we quickly overview salient details. The HM flux model is largely based on the so-called *conversion method*, whereby one inverts measured isotopic fission $\beta$ spectra (Von Feilitzsch *et al* 1982, Schreckenbach *et al* 1985, Hahn *et al* 1989) to infer the corresponding $\overline{\nu}_e$ spectra. One could instead calculate the spectrum by direct *summation* of available nuclear data. In

**Table 2.** The ratio $R$ of measured antineutrino rates compared to the predictions from various flux models, adapted from Giunti *et al* (2022). Also shown are the corresponding statistical significances and the $2\sigma$ limit on $\sin^2 2\theta_{ee}$ in the large-$\Delta m^2_{41}$ ($\gtrsim 5$ eV$^2$) region.

| Flux model | $R$ | Significance | $2\sigma$ limit on $\sin^2 2\theta_{ee}$ |
|---|---|---|---|
| HM | $0.930^{+0.024}_{-0.023}$ | $2.8\sigma$ | [0.031, 0.236] |
| EF | $0.975^{+0.032}_{-0.030}$ | $0.8\sigma$ | $<0.170$ |
| HKSS | $0.922^{+0.024}_{-0.023}$ | $3.0\sigma$ | [0.039, 0.259] |
| KI | $0.970 \pm 0.021$ | $1.4\sigma$ | $<0.144$ |
| HKSS-KI | $0.960^{+0.022}_{-0.021}$ | $1.8\sigma$ | $<0.166$ |

2019, two new, notable flux calculations appeared. The first (Estienne *et al* 2019) (hereafter 'EF') provided an updated summation calculation, while the second (Hayen *et al* 2019) ('HKSS') incorporated conversion techniques while accounting for shape alterations contributed by forbidden beta decays. The EF model predicted a $^{235}$U flux that is 5%–10% less than HM, whereas HKSS predicted a modest ($\approx$1%–2%) excess. These models have been compared with reactor rate data in (Berryman and Huber 2020, 2021, Giunti *et al* 2020, 2022); the results of Giunti *et al* (2022) are given in table 2. Interestingly, the EF model does not indicate anomalous disappearance, whereas the HKSS model slightly enhances the RAA.

The ratio of the $\beta$ spectra of $^{235}$U and $^{239}$Pu was recently measured at the Kurchatov Institute (Kopeikin *et al* 2021, 2021). In Kopeikin *et al* (2021), the $\overline{\nu}_e$ spectrum for $^{235}$U was rederived via $\beta$ conversion assuming that the $^{239}$Pu spectrum is given by the HM model; we call this 'KI.' Moreover, Giunti *et al* (2022) derives yet another flux model by rescaling the HKSS prediction for $^{235}$U by the same multiplicative factor ($1.054 \pm 0.002$) by which the integrated $^{235}$U fluxes for HM and KI disagree; the result is named 'HKSS-KI.' The experimental deficits with respect to these models are given in table 2; they are consistent with EF in that they also do not indicate significant, anomalous disappearance.

It is too soon to consider the RAA definitively resolved by these findings. For example, if one had instead assumed that the HM $^{235}$U spectrum is correct and that the $^{239}$Pu one is not, then one would find *increased* evidence for anomalous disappearance (Giunti *et al* 2017, 2019). Still, these results indicate that the conversion and summation approaches may be converging, which is a decided improvement relative to the past decade. However, the RAA is not the only motivating factor for nonstandard oscillation searches at nuclear reactors. Anomalous $\nu_e/\overline{\nu}_e$ appearance results at LSND (Aguilar *et al* 2001) and MiniBooNE (Aguilar-Arevalo *et al* 2013, 2018, 2021) and Gallium Anomaly disappearance results can still be explained in terms of an eV-scale sterile neutrino (Maltoni and Schwetz 2007, Giunti and Laveder 2010, 2011a, Kopp *et al* 2013, Dentler *et al* 2017, 2018, Gariazzo *et al* 2017, Diaz *et al* 2020). If true for LSND and MiniBooNE, then this would require nonstandard contributions to both $\nu_\mu$ and $\nu_e$ disappearance. Assuming that the central value model predictions of table 2 accurately reflect reality, flux models can still accomodate a $\sim$5%–10% change in the antineutrino rate; thus, there is still room for active-sterile mixings of modest size in the reactor sector, even without the RAA.

### *5.2. Reactor spectrum ratio experiments and the complex current landscape*

If one measures the *spectrum* of antineutrinos instead of the energy-integrated rate, then one can potentially observe oscillations directly. Moreover, if one measures the spectrum at two

**Table 3.** A tabulation of IBD-based reactor experiments that were either performed in roughly the last decade or will be performed in the near future. Experiments are sorted into short, medium, and long-baseline categories.

| Experiment | $L$ [m] | $P_{\text{th}}$ [MW] | Material(s) |
|---|---|---|---|
| DANSS (Alekseev *et al* 2018) | $\sim 11-13$ | 3100 | SS |
| MiniCHANDLER (Haghighat *et al* 2020) | 25 | 2900 | SS |
| NEOS (Ko *et al* 2017) | 24 | 2800 | LS |
| NEOS-II (Ko *et al* 2017) | 24 | 2800 | LS |
| Neutrino-4 (Serebrov *et al* 2019) | $\sim 6-12$ | 100 | LS |
| PROSPECT (Ashenfelter *et al* 2018) | $\sim 7-9$ | 85 | LS |
| PROSPECT-II (PROSPECT Collaboration 2020a) | $\sim 7-9$ | 85 | LS |
| SoLid (Abreu *et al* 2017) | $\sim 6-9$ | 40-100 | SS |
| STEREO (Almazán *et al* 2018) | $\sim 9-11$ | 58 | LS |
| JUNO-TAO (Abusleme *et al* 2020) | $\sim 30$ | 4600 | LS |
| Daya Bay (An *et al* 2016c) | 550, 1650 | 17,400 | LS |
| Double Chooz (de Kerret *et al* 2020) | 400, 1050 | 8500 | LS |
| RENO (Choi *et al* 2016) | 430, 1450 | 16,800 | LS |
| JUNO (Abusleme *et al* 2021) | 52,500 | 26,600 | LS |

(or more) baselines, then their *ratio* is largely insensitive to the details of the underlying flux model. Antineutrino spectra had been measured prior to the 2010s at, e.g. ILL (Kwon *et al* 1981, Hoummada *et al* 1995) and Bugey (Declais *et al* 1995)—these were considered in (Mention *et al* 2011)—but this program blossomed as a result of searches for nonzero $\theta_{13}$. Daya Bay, Double Chooz and RENO all employed detectors at multiple locations at the ∼km scale, as appropriate for $\Delta m^2_{31}$, but these were situated at too long a baseline to probe oscillations at the eV scale. However, experiments exploiting some combination of (1) multiple detectors, (2) movable detectors, or (3) segmented detectors have been constructed at short baselines—within 25 m—to search for eV-scale oscillations. Over the past decade, SBL searches have been performed by DANSS (Alekseev *et al* 2018), NEOS (Ko *et al* 2017), Neutrino-4 (Serebrov *et al* 2019, 2021), PROSPECT (Ashenfelter *et al* 2018, Andriamirado *et al* 2021a) and STEREO (Almazán *et al* 2018, 2020b); similar searches are ongoing at NEOS-II (Ko 2016) and SoLid (Abreu *et al* 2017). Past global analyses of reactor spectral ratios (Gariazzo *et al* 2017, Dentler *et al* 2017, Gariazzo *et al* 2018, Dentler *et al* 2018, Diaz *et al* 2020, Berryman and Huber 2020, Giunti *et al* 2020, Berryman and Huber 2021) have inferred a preference for new oscillations as high as $\gtrsim 3\sigma$, but a combination of more data and improved statistical treatments (Feldman and Cousins 1998, Agostini and Neumair 2020, Andriamirado *et al* 2020, Coloma *et al* 2021, Giunti *et al* 2021) suggests that this is no more than 1–2$\sigma$ (Giunti 2020, Berryman *et al* 2022). The 2$\sigma$ C.L. exclusion curve from a global fit of SBL spectral measurements (Berryman *et al* 2022) is shown in magenta in figure 7 (left). In comparison, Daya Bay and Bugey-3 were studied jointly in (Adamson *et al* 2020b); the result (90% $\text{CL}_s$) is shown in cyan.[16] It is a triumph of experiment that the field has matured to the point of percent-level oscillation sensitivities over the course of roughly a decade.

It is pertinent to consider how reactors fit into the landscape of $\nu_e/\overline{\nu}_e$ disappearance studies, and of sterile neutrino searches more broadly. In figure 7 (left), we show constraints on

[16] Neither of these experiments is considered in (Berryman *et al* 2022); the figure is thus not double-counting reactor spectra information.

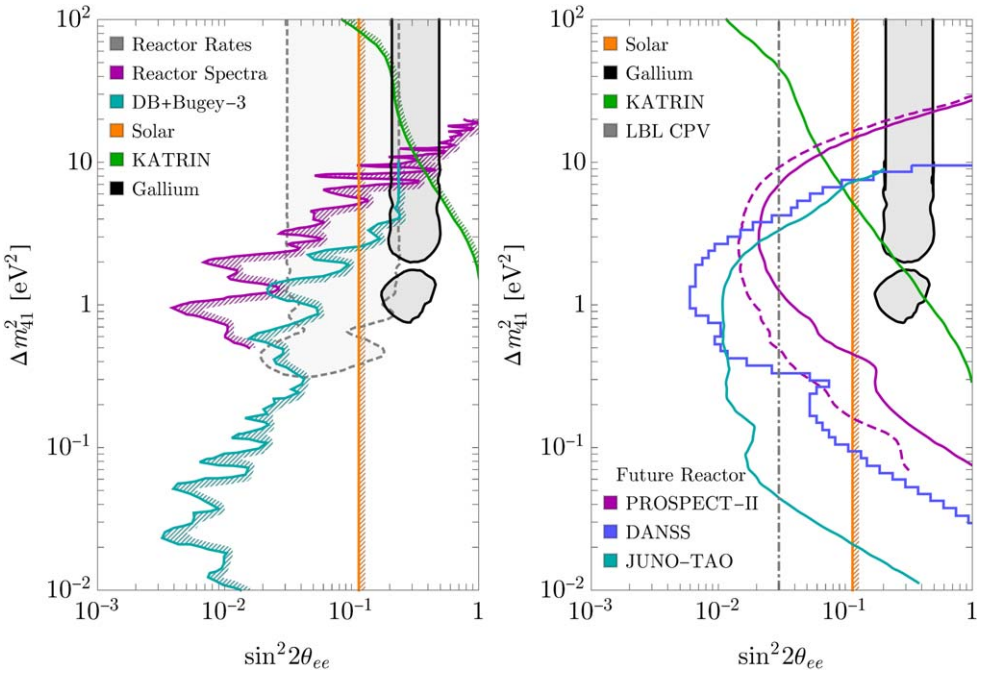


**Figure 7.** Left: Current constraints on a sterile neutrino from $\nu_e/\overline{\nu}_e$ disappearance. Color fillings represent preferences; hatching represents exclusions. The dashed, gray region is the fit to reactor rate deficits using the HM flux model (Giunti *et al* 2022), given for context. See text for more details. Right: The future sensitivities of KATRIN (Aker *et al* 2022) (green; 95% C.L.), PROSPECT-II (Andriamirado *et al* 2022) (purple; 90% C.L.), DANSS (light blue; 90% CL$_s$) and JUNO-TAO (Abusleme *et al* 2020) (cyan; 90% CL$_s$). For PROSPECT-II, two configurations are shown: two years at an HEU core (solid), and four years at an HEU core plus two years at an LEU core (dashed). The dot-dashed gray line is the *CP* violation disambiguation limit relevant for DUNE (Dutta *et al* 2016).

$\sin^2 2\theta_{ee}$ from solar neutrino experiments (Goldhagen *et al* 2022) (orange; $2\sigma$)[17] and from KATRIN (Aker *et al* 2022) (green; 95% C.L.). The region preferred ($2\sigma$) by a combined analysis of gallium experiments (Berryman *et al* 2022) is shaded in gray. In addition to SAGE and GALLEX, this includes recent results from BEST (Barinov *et al* 2022a, 2022b), where a $\gtrsim 5\sigma$ deficit has been reported (Barinov and Gorbunov 2021). Constraints have also been derived from $\nu_e$ scattering on $^{12}$C at KARMEN and LSND (Armbruster *et al* 1998, Auerbach *et al* 2001, Conrad and Shaevitz 2012), as well as from T2K (Abe *et al* 2015) and MicroBooNE (Denton 2022, Argüelles *et al* 2022); these have been omitted for clarity. Curiously, the solar constraint and the gallium preference are in $\gtrsim 3\sigma$ tension (Berryman *et al* 2022); reactor spectral measurements are compatible with either, while the compatibility between gallium and reactor rates is, as described above, flux-model dependent (Giunti *et al* 2022). Moreover, there are no significant indications of anomalous $\nu_\mu$ disappearance (Adamson *et al* 2020a); when combined with $\nu_e$ disappearance null results, this results in significant tension with the LSND and MicroBooNE anomalies (Kopp *et al* 2013, Adamson *et al* 2020b,

[17] This constraint assumes the GS98 solar model (Vinyoles *et al* 2017); had the AGSS09 solar model (Vinyoles *et al* 2017) been used, the resulting constraint would be modestly stronger.

Dentler *et al* 2018). On top of all of this, eV-scale sterile neutrinos contribute to $N_{\rm eff}$ and $\sum m_\nu$; cosmological observations place severe limits on nonstandard contributions to these quantities, disfavoring essentially all of the parameter space shown in figure 7 (Enqvist and Kainulainen 1992, Melchiorri *et al* 2009, Hannestad *et al* 2012, Archidiacono *et al* 2013, Mirizzi *et al* 2013, Gariazzo *et al* 2013, Bridle *et al* 2017, Feng *et al* 2017, Knee *et al* 2019, Berryman 2019, Gariazzo *et al* 2019, Adams *et al* 2020, Hagstotz *et al* 2021). This all suggests that $3 + 1$ oscillations do not comfortably describe the data. The question becomes: Is there a compelling conventional or BSM alternative?

The next-simplest model one could invoke would be to introduce multiple species of sterile neutrinos. This has been studied in, e.g. (Kopp *et al* 2011, Conrad *et al* 2013, Kopp *et al* 2013, Diaz *et al* 2020); including only additional oscillation frequencies does not appreciably resolve these tensions. Other proposed scenarios include sterile neutrino decay (Dentler *et al* 2020, de Gouvêa *et al* 2020), the presence of nonstandard interactions among either the active or sterile neutrinos (Liao *et al* 2019, Bhupal Dev *et al* 2019, Denton *et al* 2019), hidden sector couplings to neutrinos (Batell *et al* 2009), or some combination of multiple effects (Moss *et al* 2018). Reactor experiments will play an essential part in a necessarily diverse global program to assessing which (if any) of these scenarios are correct. As noted in section 2, they provide a clean environment in which to study oscillations, owing to (1) the flavor purity of the source; (2) the low energies, which prevent heavy states from polluting the observed signal; and (3) the relative absence of matter effects. If the existing SBL anomalies persist, and are confirmed at, e.g. the SBN program at Fermilab (Antonello *et al* 2015) and more robust future iterations of the BEST radiochemical experiment, then reactor experiments will continue to play an important role in discriminating between possible explanations thereof. The use of multiple arms of the global neutrino program to elucidate a more complex 'non-vanilla' sterile sector is very well-illustrated in (Moss *et al* 2018): in this example, which envisions a 2-component sterile sector, short-baseline reactor data is crucial for constraining active-sterile oscillation parameters, while short-baseline accelerator experiments are best at pinning down radiative decay phenomena experienced by the heavier sterile state.

As noted below equation (6), introducing a sterile neutrino also introduces two new *CP*-violating phases, which enriches the possibilities for *CP*-violation studies at long-baseline accelerator experiments. On one hand, $3 + 1$ oscillations that violate *CP* may be confounded with *CP*-conserving, $3 + 0$ oscillations (Gandhi *et al* 2015); on the other, large-amplitude, *CP*-conserving oscillations with a sterile neutrino may generate false signals of *CP* violation at, e.g. DUNE (de Gouvêa *el al* 2016). While $P_{ee}$ in equation (7) is necessarily *CP*-conserving, the sensitivity of reactors to the existence of additional neutrinos is crucial for the disambiguation of such a signature. This potential parameter degeneracy can broken if $\sin^2 2\theta_{ee}$ can be measured at the level $\lesssim$0.03 (Dutta *et al* 2016), shown by the dot-dashed line in figure 7.

### 5.3. The future of short-baseline reactor experiments

As of 2022, at least four new short-baseline reactor neutrino detectors are in preparation or under construction, with plans to address the open questions described above (table 3). The JUNO-TAO detector, a satellite detector for JUNO, will begin taking data in 2023 at a baseline of ∼30 m from a commercial power reactor in China (Abusleme *et al* 2020). The PROSPECT-II detector, a planned upgrade of the PROSPECT detector, anticipates taking a second run of data within 10m of the HFIR reactor in the US and possibly at other sites (Andriamirado *et al* 2022). The DANSS Collaboration is currently upgrading their detector to

improve their photostatistics, and thus their energy resolution (Danilov 2021). The Neutrino-4 Collaboration is also preparing an upgrade: a combination of increasing the detector volume and introducing pulse-shape discrimination is expected to triple their statistics, though the impact on their sterile neutrino sensitivity has not yet been made public (Fomin 2021). Each of these experiments will extend sensitivity to non-standard neutrino oscillation well beyond current limits, into regions of interest for the still-unresolved gallium anomaly and the continuing tension between short-baseline accelerator results. These experiments are likely to provide particularly good sensitivity in the $\sim$2–20 eV$^2$ mass splitting region, where current limits on active-sterile mixing are comparatively weaker in the electron disappearance channel. While probing this region, JUNO-TAO, PROSPECT-II and DANSS will also be able to authoritatively address existing claims of moderate confidence-level observations of sterile neutrino oscillations at the Neutrino-4 experiment (Serebrov *et al* 2021). These detectors will also increase the precision of neutrino spectrum measurements, described more in section 7.

As the neutrino community seeks to resolve remaining short-baseline neutrino anomalies, reactor experiments such as PROSPECT-II and JUNO-TAO provide several points of complementarity to other approaches. As shown in figure 7, the projected PROSPECT-II sensitivity will combine with the projected KATRIN sensitivity to fully cover the parameter space favored by the current gallium anomaly (which, as noted above, is already disfavored solar experiments) and to definitively exclude an oscillation solution to the RAA. Although the curves in figure 7 correspond most directly to a 3 + 1 sterile neutrino models, they illustrate the general point that reactor neutrinos explore a flavor channel (pure $\nu_e$) where there may not be input from other sources. They do so with relatively low cost compared to accelerator experiments, because the reactor sources are already in operation and the detector size can be on the meter-scale.

In addition to JUNO-TAO, PROSPECT-II, DANSS and Neutrino-4, which all use IBD interactions in scintillator as the detector channel, a growing number of experiments are seeking to measure CEvNS interactions at reactor sources. Ongoing reactor CEvNS projects are listed in table 4. Compared to the established IBD channel, the CEvNS signal presents a much greater experimental challenge due to high sensitivity to radiation and instrumental background. So far, the low-energy CEvNS signal has not been detected above the large backgrounds to this approach. When it becomes visible, the CEvNS signal will provide information about reactor neutrino fluxes and interactions below the IBD threshold and, like IBD searches, complement accelerator- and DAR-based searches for sterile neutrino oscillations. These experiments are discussed in more detail in sections 6 and 8.

### *5.4. Medium- and long-baseline reactor experiments*

We conclude this section by commenting on searches for nonstandard oscillations at medium- and long-baseline reactor experiments. In figure 7, we have already noted the combined constraint from Daya Bay and Bugey-3 (Adamson *et al* 2020b); the constraint is dominated by Daya Bay below $\Delta m^2_{41} \lesssim 0.3$ eV$^2$. Similar exclusions have been derived for RENO and Double Chooz (Abrahão *et al* 2021a, Choi *et al* 2020a). Long-baseline experiments are sensitive to smaller values of $\Delta m^2_{41}$ than those shown in figure 7: the JUNO collaboration forecasts a sensitivity to $\sin^2 2\theta_{ee} \gtrsim 0.02$ for $3 \times 10^{-4} \lesssim \Delta m^2_{41} \lesssim 2 \times 10^{-3}$ (An *et al* 2016a).

Neutrino oscillations are fundamentally contingent on the coherence of the neutrino wavepacket; decoherence could dramatically change the oscillation probabilities at medium and long baselines. The Daya Bay Collaboration has studied these effects in (An *et al* 2017a) and

**Table 4.** A tabulation of CE$\nu$NS reactor experiments, including their reactor standoff $L$, the reactor (thermal) power $P_{\text{th}}$, component material(s) and detection technology.

| Experiment | $L$ [m] | $P_{\text{th}}$ [MW] | Material(s) | Technology |
|---|---|---|---|---|
| CHILLAX (Xu 2021) | ∼25 | ∼1000 | LAr and LXe | Dual-Phase TPC |
| CONNIE (Aguilar-Arevalo *et al* 2019, 2022) | 30 | 3800 | Si | Skipper CCDs |
| CONUS (Bonet *et al* 2021a) | 17 | 3900 | Ge | Ionization |
| MINER (Agnolet *et al* 2017) | ∼2–10 | 1 | Ge, SI, $Al_2O_3$ | Bolometry |
| NCC-1701 (Colaresi *et al* 2021) | 8 | 2960 | Ge | Ionization |
| NEON (Choi *et al* 2020b) | 24 | 2800 | NaI(Tl) | Scintillation |
| NEWS-G (Vidal 2020) | ⋯ | ⋯ | Ne | Ionization |
| $\nu$GeN (Belov *et al* 2015) | ∼10 | 3100 | Ge | Ionization |
| NUCLEUS (Angloher *et al* 2019) | ⋯ | ⋯ | $CaWO_4$ and $Al_2O_3$ | Bolometry |
| NUXE (Ni 2020, Ni *et al* 2021) | ∼25 | ∼3000 | LXe | Ionization/ Scintillation |
| RED-100 (Akimov *et al* 2017) | 19 | 3100 | LXe | Dual-Phase TPC |
| Ricochet (Billard *et al* 2017, Augier *et al* 2021) | 8.8 | 58 | Ge and Zn | Bolometry |
| SBC (Flores *et al* 2021) | 3 | 1 | LXe | Scintillation |
| TEXONO (Kerman *et al* 2016, Sharma *et al* 2021) | 28 | 2900 | Ge | Ionization |
| $\nu$IOLETA (Moroni 2021) | 8, 12 | 2000 | Si | Skipper CCDs |

finds that they are not significant in their existing data. This is confirmed in joint analyses of Daya Bay, RENO and KamLAND in (Gouvea *et al* 2020, Gouvêa *et al* 2021). The JUNO collaboration has benchmarked their sensitivities to several models of decoherence in (Wang *et al* 2022) (see also Gouvea *et al* 2020); they forecast approximately one order of magnitude improvement in measuring the size of the neutrino wave-packet. Decoherence effects link up with sterile neutrino searches in a nontrivial way: recent work (Argüelles *et al* 2023) finds that these can be important in correctly assessing constraints at SBL reactor experiments for $\Delta m^2_{41} \sim \mathcal{O}(\text{eV}^2)$. These findings again highlight the importance of robust reactor programs at both short and long baselines.

We finally briefly note the capabilities of longer-baseline reactor experiments in probing a wider variety of exotic BSM scenarios. A variety of such studies have been performed at high-statistics medium-baseline experiments, such as *CPT* and Lorentz-invariance violation searches at Daya Bay (Adey *et al* 2018) and Double Chooz (Abe *et al* 2012a). Other exotic studies, such as searches for large extra dimensions have also been proposed (Basto-Gonzalez *et al* 2022).

## 6. Probing neutrino properties and unknown particles with reactors neutrino detectors

### *6.1. Reactor CE$\nu$NS and low-energy processes: theory and experimental limits*

CE$\nu$NS is a neutral-current process that arises when the momentum transfer in the neutrino-nucleus interaction is less than the inverse of the size of the nucleus. For typical nuclei, this corresponds to neutrinos with energies $E_\nu \lesssim 50\,\text{MeV}$. In the SM, the interaction is mediated

by the $Z$-boson, with its vector component leading to the coherent enhancement. As a reference point, we first write the cross section in the form

$$\frac{\mathrm{d}\sigma}{\mathrm{d}T} = \frac{G_{\mathrm{F}}^2 M}{4\pi}\left(1 - \frac{MT}{2E_\nu^2}\right) Q_{\mathrm{w}}^2 [F_{\mathrm{w}}(q^2)]^2, \tag{8}$$

where $G_{\mathrm{F}}$ is the Fermi constant, $T = E_R = q^2/(2M) = E_\nu - E_\nu'$ is the nuclear recoil energy (taking values in $[0,\ 2E_\nu^2/(M + 2E_\nu)]$), $F_{\mathrm{w}}(q^2)$ is the weak form factor, $M$ is the mass of the target nucleus, and $E_\nu$ ($E_\nu'$) is the energy of the incoming (outgoing) neutrino. The tree-level weak charge is defined by

$$Q_{\mathrm{w}} = Z(1 - 4\sin^2\theta_W) - N, \tag{9}$$

with proton number $Z$, neutron number $N$, and weak mixing angle $\sin^2\theta_W$. To first approximation, the weak form factor $F_{\mathrm{w}}(q^2)$ depends on the nuclear density distribution of protons and neutrons. In the coherence limit $q^2 \to 0$ it is normalized to $F_{\mathrm{w}}(0) = 1$, with the coherent enhancement of the cross section reflected by the scaling with $N^2$ via the weak charge, given the accidental suppression of the proton weak charge $Q_{\mathrm{w}}^p \ll 1$. Consequently, this implies that CE$\nu$NS is mainly sensitive to the neutron distribution in the nucleus.

Nuclear reactors have long been utilized as copious sources of electron anti-neutrinos. Neutrinos from reactors have been detected using the IBD reaction, $\bar{\nu}_e + p{+}1.806$ MeV $\rightarrow e^+ + n$, by observing both the outgoing positron and coincident neutron. The characteristic neutrino energy for this source is $\lesssim$1 MeV, roughly an order of magnitude or more lower than the average energies of neutrinos produced by accelerator sources. Due to these low energies, the coherence condition for the recoil is largely preserved over the entire reactor energy regime, so that there is no dependence on the internal structure of the nucleus.

In general, the presence of any BSM physics will modify the previous cross sections, thus altering the expected number of events detected via the CEvNS reaction in a detector. In a general fashion, we write the total cross section in the presence of BSM as

$$\frac{\mathrm{d}\sigma}{\mathrm{d}E_R} = \left.\frac{\mathrm{d}\sigma}{\mathrm{d}E_R}\right|_{\mathrm{SM}} + \left.\frac{\mathrm{d}\sigma}{\mathrm{d}E_R}\right|_{\mathrm{BSM}}, \tag{10}$$

where the first term is the SM cross section for either neutrino-electron and CE$\nu$NS interactions, and the second is the modification created by the BSM interactions. Note that any possible interference effect that can appear according to the nature of the new mediators are included in the BSM cross section.

The new physics can be enhanced by light mediators. It could be the photon coupling through electromagnetic properties of the neutrino, or additional mediators having couplings to neutrinos, charged leptons and quarks. In the spirit of simplified models, we assume a Lagrangian at low energies which includes terms for the new interactions with the SM fermions without specifying the gauge invariant models at high energies as in Fernandez-Moroni *et al* (2021). For each scenario, the modification of both neutrino-electron and CE$\nu$NS cross sections will have a specific shape, possibly including interference effects. In table 5 we summarize and compile the distinct BSM contributions to the neutrino-electron and CE$\nu$-NScross sections for each light mediator scenario, together with the non-zero couplings relevant in each case.

In the specific case of CE$\nu$NS, there is an additional step; we need to translate the interactions from the quark to the nucleon level. The coherence factors related to the specific mediator are given by see e.g. Alarcon *et al* (2012), (2014), Cirelli *et al* (2013), Hill and Mikhail (2015), Cerdeno *et al* (2016)

**Table 5.** Contributions to the neutrino-electron and CE$\nu$NS cross-sections for the different scenarios considered here. The $g_V$, $g_A$ are given by $g_V = \frac{1}{2} + 2\sin^2\theta_W$, $g_A = \frac{1}{2}$ (Cerdeno *et al* 2016).

| Interaction | Non-zero couplings | $\frac{d\sigma_{\nu e}}{dE_R}\Big\vert_{BSM}$ | $\frac{d\sigma_{CE\nu NS}}{dE_R}\Big\vert_{BSM}$ |
|---|---|---|---|
| Magnetic moment | $\mu_{\nu_e}$ | $\alpha_{EM}\mu^2_{\nu_e}\frac{E_\nu - E_R}{E_\nu E_R}$ | $\alpha_{EM}\mu^2_{\nu_e} Z^2 \frac{E_\nu - E_R}{E_\nu E_R}\mathcal{F}^2(E_R)$ |
| Scalar | $g_{\nu,\phi}$, $g_{es}$, $g_{qs}$ | $\frac{g^2_{\nu,\phi}g^2_{es}E_R m_e^2}{4\pi E_\nu^2(2E_R m_e + m_\phi^2)^2}$ | $\frac{Q_S^2 m_N^2 E_R g^2_{\nu\phi} g^2_{qs}}{4\pi E_\nu^2(2E_R m_N + m_\phi^2)^2}$ |
| Pseudoscalar | $g_{\nu,\phi}$, $g_{ep}$, $g_{qp}$ | $\frac{g^2_{\nu,\phi}g^2_{ep}E_R^2 m_e}{8\pi E_\nu^2(2E_R m_e + m_\phi^2)^2}$ | 0 |
| Vector | $g_{\nu Z'}$, $g_{ev}$, $g_{qv}$ | $\frac{\sqrt{2}G_F m_e g_V g_{\nu Z'} g_{ev}}{\pi(2E_R m_e + m^2_{Z'})}$ $+\frac{g^2_{\nu Z'}g^2_{ev}m_e}{2\pi(2E_R m_e + m^2_{Z'})^2}$ | $-\frac{G_F m_N Q_V^{SM} Q'_V (2E_\nu^2 - E_R m_N)}{2\sqrt{2}\pi E_\nu^2(2E_R m_N + m^2_{Z'})}$ $+\frac{Q'^2_V m_N (2E_\nu^2 - E_R m_N)}{4\pi E_\nu^2(2E_R m_N + m^2_{Z'})^2}$ |
| Axial | $g_{\nu Z'}$, $g_{ea}$, $g_{qa}$ | $-\frac{\sqrt{2}G_F m_e g_A g_{\nu Z'} g_{ea}}{\pi(2E_R m_e + m^2_{Z'})}$ $+\frac{g^2_{\nu Z'}g^2_{ea}m_e}{2\pi(2E_R m_e + m^2_{Z'})^2}$ | $\frac{G_F m_N Q_A Q'_A (2E_\nu^2 + E_R m_N)}{2\sqrt{2}\pi E_\nu^2(2E_R m_N + m^2_{Z'})}$ $-\frac{G_F m_N Q_V^{SM} Q'_A E_\nu E_R}{2\sqrt{2}\pi E_\nu^2(2E_R m_N + m^2_{Z'})}$ $+\frac{Q'^2_A m_N (2E_\nu^2 + E_R m_N)}{4\pi E_\nu^2(2E_R m_N + m^2_{Z'})^2}$ |

$$Q'_V = 3(N+Z)g_{\nu Z'}g_{qv}, \tag{11a}$$

$$Q'_A = 0.3 S_N g_{\nu Z'} g_{qa}, \tag{11b}$$

$$Q_A = 1.3 S_N, \tag{11c}$$

$$Q_S = 14(N+Z) + 1.1Z, \tag{11d}$$

corresponding to the vector, axial, SM axial, and scalar currents, with nuclear spin $S_N$, and neutrino-$Z'$ and quark vector couplings $g_{\nu Z'}$ and $g_{qv}$, respectively.

Figure 8 shows the sensitivity at 90% C.L. of a new light scalar mediator coupling to neutrinos and quarks (left panel) and the sensitivity to a light vector mediator coupled to neutrinos and quarks (right panel), for current experiments using accelerator neutrinos (blue area) and reactor neutrinos (green area) (Aguilar-Arevalo *et al* 2020, Colaresi *et al* 2021). New sensor technologies aiming to detect CEvNS at nuclear reactors have thresholds low enough to reap the benefits of the large neutrino flux of the reactor and access these new physics models. Both graphs show a better sensitivity for mediator masses below 20MeV in reactor-based CEvNS experiments. The projected sensitivity for a 10 kg experiment using Skipper CCD (Tiffenberg *et al* 2017b) with silicon as the target material is also shown in both plots. The sensor allows for a energy threshold of a few eV of the equivalent ionization energy. A wide range of coupling constants is unconstrained in the parameter space for masses for light mediators (Fernandez-Moroni *et al* 2021). Since the interaction cross sections scale with the fourth power of the coupling parameter ($y$-axes in the plots), the increase in sensitivity of this new search is several orders of magnitude of the existing limits.

The combination of three aspects—the cross-section enhancement for nuclear interaction for the reactor neutrino energies, the very low energy threshold of new technologies to observe faint depositions, and the reactor being the most intense neutrino flux on earth—make the proposed technique a unique tool to search for dark sector candidates in new regimes.

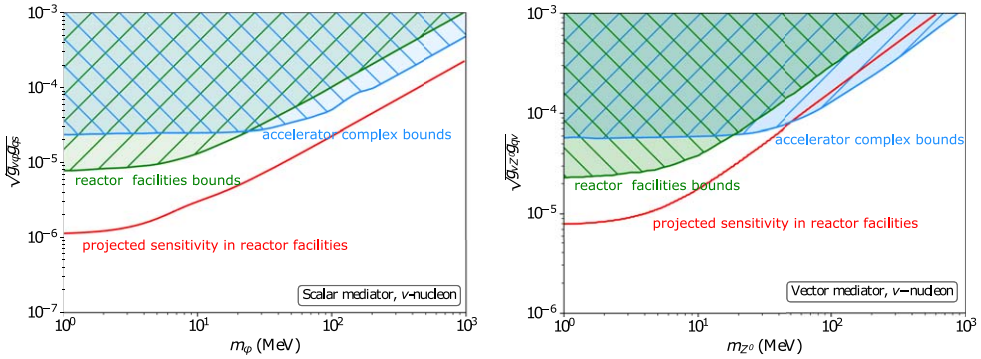


**Figure 8.** Current bounds and projected sensitivity bounds for new neutrino interactions with nucleons through a scalar mediator (left) and vector mediator (right). Plots show with different colors the parameter space ruled out using neutrinos from accelerator complex and neutrinos from nuclear reactor facilities. Figures taken from Fernandez-Moroni *et al* (2021).

### *6.2. Experimental requirements for reactor CEνNS detection*

The maximum nuclear recoil energy resulting from CEvNS interactions can be approximated as $2k^2/M$, and is usually at the keV level or below for reactor antineutrinos with a characteristic energy of $\lesssim$1 MeV. As illustrated in figure 9, with a Si/Ar/Ge/Xe target, 90% of the reactor CEvNS signals will have an energy below 0.8/0.6/0.3/0.2 keV. In addition, the majority of energy transferred from the antineutrino to a nucleus is dissipated as heat. As a result, for detector technologies that measure scintillation and/or ionization signatures from particle interactions, only a small fraction of nuclear recoil energy is observable. In Si (Chavarria 2016), Ge (Jones and Kraner 1975, Scholz *et al* 2016, Bonhomme *et al* 2022) and Xe (Lenardo *et al* 2019) the reduction factors of measurable energy (or quenching factors) have been measured down to ∼0.3 keV, with typical suppression values around 6–10 in this energy regime. This quenching effect, in addition to the low nuclear recoil energy, makes the detection of reactor CEvNS signals challenging.

Thanks to the progress of direct detection dark matter experiments in the last few decades, low-threshold detectors sensitive to keV-level nuclear recoils have been developed (Aprile *et al* 2019, Amaral *et al* 2020, Aguilar-Arevalo *et al* 2020b, Barak *et al* 2020). A typical dark matter experiment focuses on nuclear recoils from a few keV to tens of keV, and thus the detection of reactor CEvNS requires the detector thresholds to be further reduced. Several experimental efforts have been launched to advance the low-energy sensitivity of detector technologies including Si and Ge ionization detectors (Amaral *et al* 2020, Barak *et al* 2020, Bonet *et al* 2021a, Aguilar-Arevalo *et al* 2022), liquid argon and xenon scintillation/ionization detectors (Akimov *et al* 2017, Agnes *et al* 2018, Aprile *et al* 2019, Ni 2020, Flores *et al* 2021, Xu 2021), and cryogenic bolometers (Agnolet *et al* 2017, Strauss *et al* 2017, Abdelhameed *et al* 2019, Augier *et al* 2021). To date, energy thresholds in the range of tens of eV to hundreds of eV have been demonstrated in bolometers and ionization detectors.

Coincidentally, at a detection threshold of ∼200 eV, reactor CEvNS experiments using different targets are expected to observe comparable event rates per target mass (figure 9). Because of the near-exponential shape of the CEvNS spectra, an experiment with a 50 eV threshold will be able to collect 5–10 times more CEvNS events than those with 200 eV thresholds, demonstrating the need to develop lower-threshold detector technologies. Further,

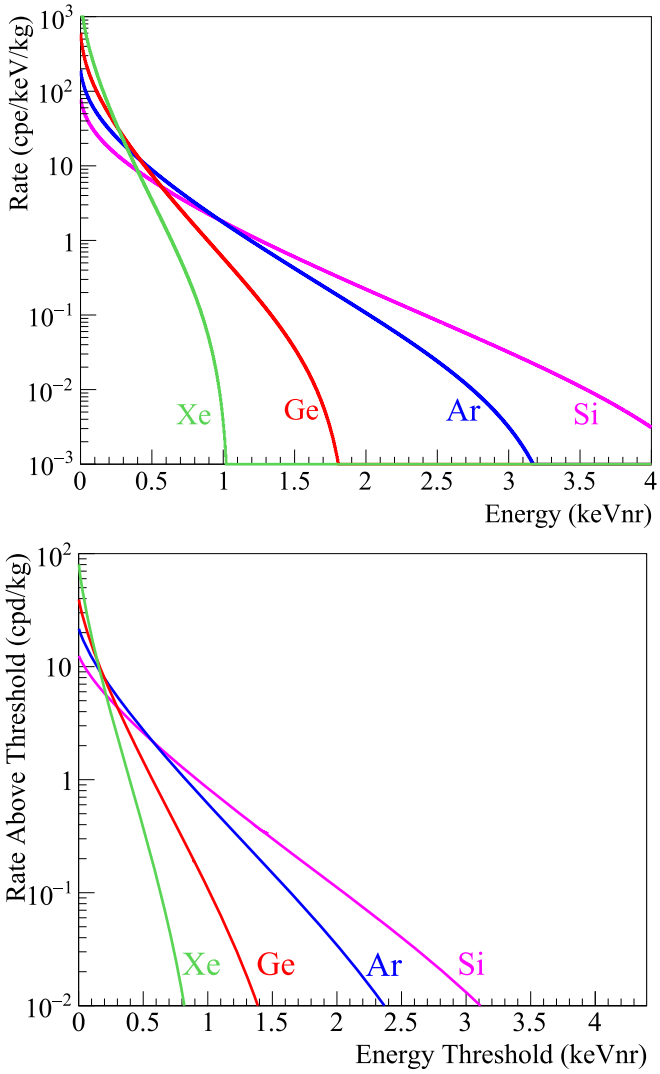


**Figure 9.** Top: the expected reactor CEvNS energy spectra in a Si/Ar/Ge/Xe target, with the assumption of 1 kg target mass and 25 m standoff distance from a 1GW reactor core; reactor antineutrino spectrum is taken from Hayes and Vogel (2016). Bottom: integrated CEvNS event rate in 1 kg of Si/Ar/Ge/Xe as a threshold of detector energy threshold, with the same assumption on reactor parameters as for the left figure.

due to the low expected event rate of neutrino interactions, a detector also needs to have a large active mass to obtain sufficient statistics to study possible BSM physics associated with CEvNS. Currently available low-threshold detectors such as Skipper CCDs are limited to active masses at a hundred-gram level (Barak *et al* 2020, Nasteva 2021), while high-mass detectors such as liquid argon and xenon Time Projection Chambers (TPCs) are limited to an energy threshold of hundreds of eV (Agnes *et al* 2018, Aprile *et al* 2019, Akerib *et al* 2021). Ongoing R&D efforts are currently pursuing substantial improvements in these directions

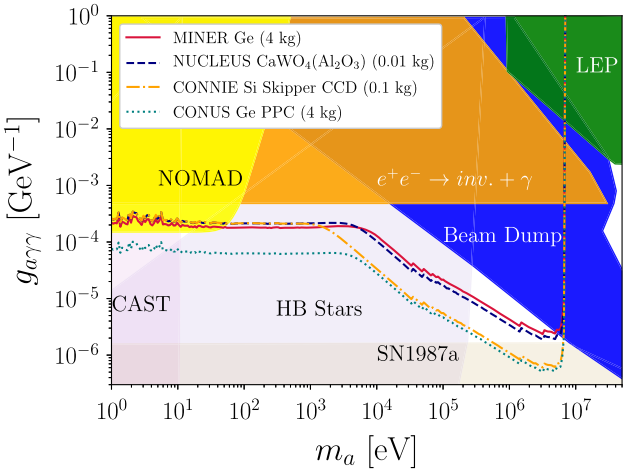


**Figure 10.** Comparison of sensitivity of axion like particles searches at nuclear reactor compared with excising bounds. Figure taken from Dent *et al* (2020).

(Lenardo *et al* 2019, Estrada 2020, Settimo 2020, Agnes *et al* 2021). More R&D is needed in the next decade to perform a first definitive experimental observation of reactor CEvNS.

In addition to detector threshold and active mass, another important aspect to consider in reactor CEvNS detection experiments is the excess backgrounds observed in the low energy regions of different detectors (Aprile *et al* 2019, Agnes *et al* 2018, Workshop 2021, Akerib *et al* 2020, Fuss *et al* 2022), which operate at very different temperatures and have different signal readout schemes. Such backgrounds often manifest themselves as a fast rising event rate as the energy approaches the detector threshold, and can vary drastically in rate, temporal behavior, and other characteristics. In ionization detectors these backgrounds are suspected to arise from the trap and delayed release of electrons (Agnes *et al* 2018, Akerib *et al* 2020) or low-energy interactions near the active volume (Fuss *et al* 2022), and in bolometers they are sometimes hypothesized to originate from crystal stress or accumulation of energy in the active volume (Workshop 2021, Fuss *et al* 2022). Much remains unstudied for these experiments to enjoy meaningful nuclear recoil sensitivities in the reactor CEvNS energy regime.

### *6.3. Exotic particle searches at nuclear reactors*

Other novel aspects of reactor-based experiments, such as their on-surface location and their proximity to large reactor-produced photon fluxes, can be leveraged to probe the existence of a range of hidden sector particles and interactions. Below, we illustrate with a few examples.

Nuclear reactors are also an intense source of photons and neutrons, which can interact with the materials of the reactor structure or spontaneously transform to produce hidden sector candidates that could escape from the reactor core and reach a nearby detector. This new framework of production and detection at nuclear facilities has been studied due to the large production rates obtained in reactors and the availability of new technologies to detect them (Danilov *et al* 2019, Dent *et al* 2020, Sierra *et al* 2021). As an example of the sensitivity of this technique figure 10 (from Dent *et al* 2020) shows the reach in the search for axion-like particles for different low threshold sensor technologies in nuclear reactors (different color lines) compared to other astrophysically derived constraints (shaded areas). The plot shows

the parameter space of axion-like particles coupling to photons, with coupling constant in the *y* axes and particle mass in the *x* axes. As the plot shows, the new technique shows unprecedented sensitivity to regions that cannot be accessed by other experiments for axion masses around 1 MeV—the so called 'cosmological triangle.' These detectors can also similarly detect other indirectly electron- or photon-coupled hidden sector particles generated in the core, such as millicharged particles (Singh *et al* 2019). Neutron-sensitive detectors, such as those used in reactor IBD experiments, are highly capable of probing neutron-coupled hidden sector particles; a search setting world-leading limits on hidden neutrons was recently reported by the STEREO experiment (Almazán *et al* 2022b).

Most short-baseline reactor experiments are located on-surface and lack a substantial amount of overburden. While disadvantageous from the perspective of increases in neutrino-like cosmic backgrounds, it also provides unique advantages for the detection of high-cross-section cosmogenic dark matter particles that would be otherwise attenuated before reaching a detector (Cappiello and Beacom 2019) The PROSPECT reactor antineutrino experiment has used its overburden-free, PSD-capable IBD detector to perform a sensitive search for single proton recoils from interactions of boosted dark matter in the sub-GeV mass regime (Andriamirado *et al* 2021b). Similar on-surface reactor-located rare event searches may also be applicable for pursuit of other BSM particle types, such as multiply-interacting massive particles (MIMPS) (Bramante *et al* 2018, 2019) or macroscopic dark matter (Bai and Berger 2020).

## 7. Improving reactor and nuclear physics knowledge through neutrino measurements and modelling

### *7.1. Reactor neutrino flux and spectrum measurements*

Antineutrino emissions from LEU and HEU reactors have been precisely measured by a range of IBD detection experiments covering baselines from roughly 7–2000 m. While some experiments have measured emissions from HEU reactors, which burn only $^{235}$U, most others have sampled LEU reactors, whose neutrino emissions are contributed by the primary fissile isotopes ($^{235}$U, $^{238}$U, $^{239}$Pu, and $^{241}$Pu) according to their fission fractions at a specific point in the reactor's burnup cycle. These measurements enable accurate evaluation of antineutrino yields and spectra per fission from the primary fissile isotopes, as well as providing cross-checks for antineutrino flux predictions made from nuclear databases and beta-spectra conversions.

Experiments listed in table 6 measured the IBD detection rate from various reactors with organic scintillator targets. Using precise knowledge of the rate of reactor fission in the core and the IBD detection efficiency (see An *et al* 2017b, Adey *et al* 2019a) for details), IBD rate measurements can be converted to a measure of IBD yield, or antineutrino flux times the well-known IBD cross-section (Vogel and Beacom 1999). Time-averaged IBD yield measurements made by most experiments provided a first global picture of a family of uncorrelated or modestly correlated data points from different baselines and fissile isotope compositions (Mention *et al* 2011, Zhang *et al* 2013). Among the example experiments in table 6, Bugey-4, Daya Bay, RENO and Double CHOOZ measured the IBD rate from corresponding reactors with experimental uncertainties of 1.4%, 1.5%, 2.1%, and 1.0%, respectively (Declais *et al* 1994, Adey *et al* 2019a, Bak *et al* 2019, de Kerret *et al* 2020). The examples on HEU produced IBD rate includes the ILL, Savannah River, and STEREO measurements with uncertainty of 9.1%, 2.9%, and 2.5%, respectively (Kwon *et al* 1981, Greenwood *et al* 1996, Almazán *et al* 2020a). From this dataset, IBD yields of $^{235}$U could be tightly constrained

**Table 6.** Examples of IBD experiments' measurements of reactor neutrino flux, spectrum, and evolution, with different reactor compositions.

| Experiment | $f_{235}$ | $f_{238}$ | $f_{239}$ | $f_{241}$ | Measurements |
|---|---|---|---|---|---|
| Bugey-3 | 0.614 | 0.074 | 0.274 | 0.03 | flux/spect |
| Bugey-4 | 0.614 | 0.074 | 0.274 | 0.03 | flux |
| Daya Bay | 0.630–0.511 | 0.075–0.077 | 0.253–0.345 | 0.042–0.068 | flux/evol/spect |
| RENO | 0.62–0.527 | 0.072–0.074 | 0.262–0.333 | 0.046–0.066 | flux/evol/spect |
| Double CHOOZ | 0.520 | 0.087 | 0.333 | 0.060 | flux/spect |
| ILL | 1 | 0 | 0 | 0 | flux |
| Savannah river | 1 | 0 | 0 | 0 | flux |
| STEREO | 1 | 0 | 0 | 0 | flux/spect |
| PROSPECT | 1 | 0 | 0 | 0 | spect |

using HEU measurements, while constraints on the yields of the remaining isotopes remained quite loose (Giunti 2017b).

Beyond time-integrated yields, the Daya Bay and RENO experiments more recently reported IBD yields measured at various points in their reactors' fuel cycles with the same reactor-detector configuration (An *et al* 2017c, Bak *et al* 2019), yielding a set of highly-correlated data points capable of substantially improving direct knowledge of $^{239}$Pu and $^{238}$U yields (Giunti 2017a, Gebre *et al* 2018, Giunti *et al* 2019). Best-fit isotopic IBD yields provided by time-integrated and so-called 'flux evolution' datasets are shown in figure 11.

As overviewed in table 6, many of these reactor experiments have also reported the differential spectrum of IBD positron energies detected per fission, while others have further unfolded this IBD positron spectrum into an interacting antineutrino energy spectrum per fission. Meaningful measurements of this type require detectors with positron energy resolutions roughly of order 20% or better. While first high-statistics absolute spectrum measurements at LEU reactors first became available in the mid-1990s (Achkar *et al* 1996), available precision greatly improved with the $\theta_{13}$ experiments of the 2010's (Abe *et al* 2014, An *et al* 2016c, Choi *et al* 2016). Precision HEU spectra only become available very recently with the PROSPECT and STEREO experiments (Ashenfelter *et al* 2019, Molina *et al* 2021). The interacting neutrino spectrum per fission for $^{235}$U and $^{239}$Pu was reported by Daya Bay measuring spectra at different points in its reactors' fuel cycles (Adey *et al* 2019b, An *et al* 2021). Measured $^{235}$U isotopic spectra have been demonstrated to be generally consistent between Daya Bay, PROSPECT, and STEREO (Almazán *et al* 2022a, An *et al* 2022).

### *7.2. Modeling reactor antineutrino emissions*

Two complementary methods are available for modelling the per-experiment or isotopic IBD yields and spectra per fission reported in the previous section (Hayes and Vogel 2016). The first is the 'summation' or '*ab initio*' method in which the flux and spectra are directly calculated from tabulated fission yields and branching ratios. This method uses nuclear databases, such as JEFF (Plompen *et al* 2020), to account the fission yields, as well as data on beta-unstable isotopes from ENSDF databases (Tuli 1996) to sum the theoretical beta spectra of hundreds of fission products and thousands of beta branches. Uncertainties in the summation method are contributed by missing information of beta-unstable isotopes and uncertainties of beta decay branching and fission product yields. Until very recently, tabulations also did not account for correlations in fission yield and decay uncertainties between isotopes and branches, meaning that uncertainty envelopes, even when provided, are ill-defined.

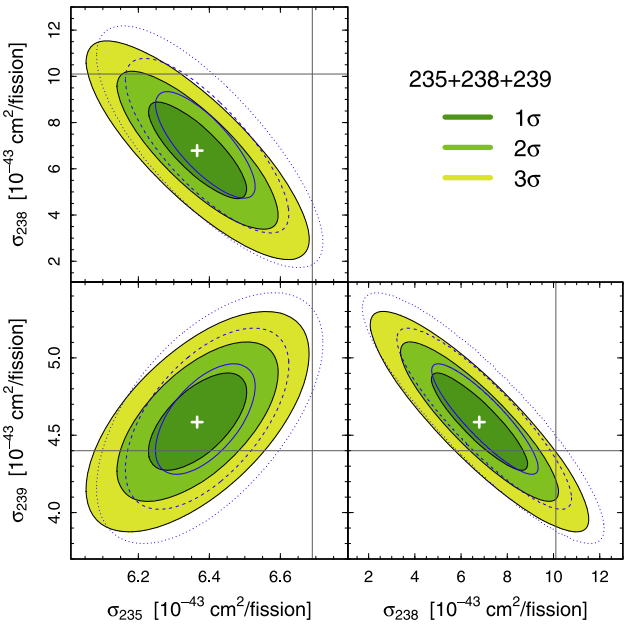


**Figure 11.** Allowed regions for isotopic IBD yields of $^{235}$U, $^{239}$Pu, and $^{238}$U provided by a fit of time-integrated and 'flux evolution' IBD yield datasets. For this fit, sterile neutrino oscillations are assumed to be negligible. Figure taken from Giunti *et al* (2019).

Recently, cataloguing of fission yield correlations (Fiorito *et al* 2014, Matthews *et al* 2021) and addition of improved decay data using total absorption spectroscopy (TAGS) techniques (Greenwood *et al* 1997, Algora *et al* 2010, Zakari-Issoufou *et al* 2015, Rasco *et al* 2016, Fijałkowska *et al* 2017, Rice *et al* 2017, Valencia *et al* 2017, Guadilla *et al* 2019a, 2019b, 2019c) has provided the promise of reducing and better understanding summation uncertainties.

The second method, generally considered to be more precise, performs the conversion of measured aggregate post-fission beta decay spectra into antineutrino spectra through the fitting of a limited number of individual beta branches (Huber 2011, Mention *et al* 2011). The universally used aggregate beta decay datasets underlying this method were measured by neutron-induced fission of $^{235}$U (Schreckenbach *et al* 1985), $^{239}$Pu (von Feilitzsch *et al* 1982), and $^{241}$Pu (Hahn *et al* 1989) at the ILL reactor. Beta-branches are fitted to the cumulative beta spectra such that the sum of branches is the best-fit to measured beta spectrum. This data-driven approach has the advantage of being immune to uncertainties from unknown or unmeasured beta decay spectra. However, the fitted branches do not fully represent the ∼1000 fission-produced beta branches actually present in the spectrum. Theoretical corrections, including forbidden transitions (Hayes *et al* 2014, Hayen *et al* 2019) and weak magnetism corrections (Wang *et al* 2016), which add additional uncertainties. Flux prediction of neutrinos from $^{238}$U, and other non-fissile isotopes in reactor facilities, still rely on other experimental data or nuclear database summation.

These two methods have complementary, largely uncorrelated uncertainties, and efforts have been taken in recent years to compare their outcomes. While the conversion and summation spectral predictions had been initially thought to be in conflict (Dwyer and

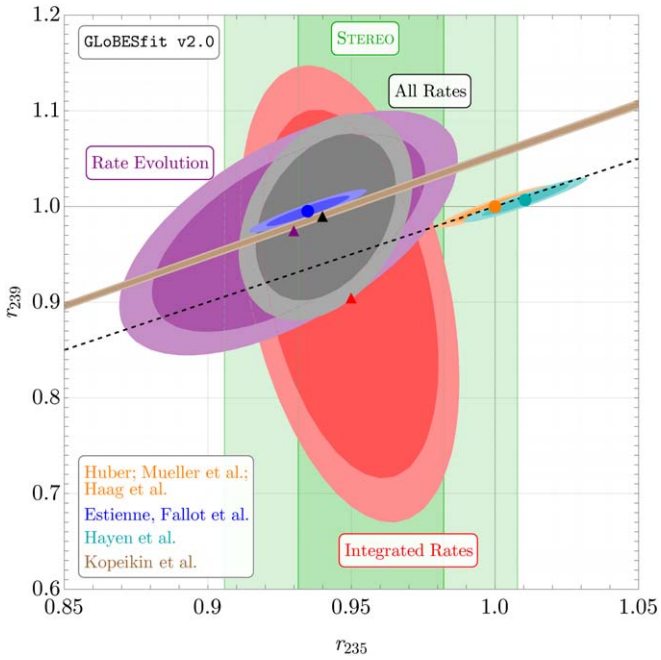


**Figure 12.** The 95% C.L. (dark) and 99% C.L. (light) contours in $r_{235}$–$r_{239}$ plane for integrated rate (red), fuel evolution (purple) and all reactor experiments (black), where $r_X$ is the ratio of the flux predicted/measured for isotope $X$ over its HM prediction. The result from STEREO (Almazán *et al* 2020a) is shown in green; the bands represent the $1\sigma$ (dark) and $2\sigma$ (light) regions. Orange, blue and cyan ellipses represent the expectations from the HM, EF and HKSS flux models, respectively; $1\sigma$ ($2\sigma$) is shown in dark (light) shades. Brown bands represent the $1\sigma$ (dark) and $2\sigma$ (light) determination of the $^{239}\mathrm{Pu}/^{235}\mathrm{U}$ ratio from the Kurchatov Institute (Kopeikin *et al* 2021, 2021). Along the black dashed line $r_{235} = r_{239}$. Triangles represent the best-fit values for the three fits, and the circles show the central values for the flux models. Figure and caption adapted from Berryman and Huber (2021).

Langford 2015, Hayes *et al* 2015), more recent studies using up-to-date database and decay information have found striking spectral shape agreement between prediction methods (Estienne *et al* 2019). On the other hand, all recent studies have found discrepancies between the methods' predicted energy-integrated fluxes, both in overall magnitude and in the relative offset between $^{235}$U and $^{239}$Pu yields (Hayes *et al* 2018, Estienne *et al* 2019, Berryman and Huber 2021). Flux model offsets are illustrated in figure 12 as the difference between blue and orange/cyan circle data points.

### *7.3. Data-model discrepancies*

With improvements in reliability of the models and precision of IBD yield and spectrum measurement in the last decade, a variety of data-model discrepancies have emerged. First, the global average of measured reactor neutrino fluxes were found to be offset with respect to the more-precise conversion prediction (Mention *et al* 2011)—the 'reactor antineutrino anomaly' described in some detail in section 5. This discrepancy is visible as the diagonal offset between the red and orange ellipses in figure 12. More recently, the flux evolution

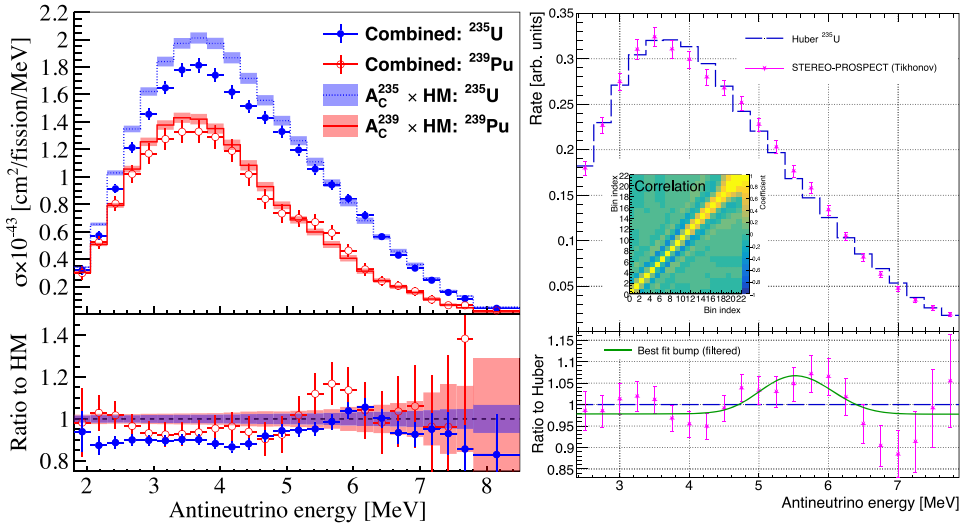


**Figure 13.** Joint unfolded interacting antineutrino energy spectrum of $^{235}$U and $^{239}$Pu from Daya Bay and PROSPECT (left) and of $^{235}$U from STEREO and PROSPECT (right). Comparisons to the Huber–Mueller model are given in both cases. From An *et al* (2022) and Almazán *et al* (2022a).

datasets from Daya Bay and RENO have elucidated that, absent neutrino oscillations, this flux anomaly can be more accurately interpreted as an offset in measured and predicted $^{235}$U IBD yields, visible as a horizontal offset between the purple and orange ellipses in figure 12. Moreover, the consonance between flux evolution datasets, summation predictions, and recent conversion predictions using new fission beta measurements (Kopeikin *et al* 2021) indicates that ILL-measured beta spectrum inputs to the conversion approach may be largely to blame for IBD yield data-model discrepancies. Historical reactor decay heat measurements have also been recently investigated towards this end (Sonzogni *et al* 2022).

Recent measurements of the antineutrino energy spectra at LEU and HEU reactors also demonstrate discrepancies between data and predictions. As demonstrated in figure 13, there is most notably an excess of events observed at approximately 5 MeV which is not matched by theoretical models. This so-called 'bump' has been the focus of much interest in the neutrino as well as the nuclear physics community, since there are only a small number of high-$Q$ isotopes which contribute the majority of neutrinos in this region (Sonzogni *et al* 2015). While this spectral deviation was first observed at LEU reactors, short-baseline measurements by PROSPECT and STEREO have observed a similar-sized effect in the spectrum of $^{235}$U, indicating a common mis-modelling of the interacting antineutrino energy spectrum of multiple fissile isotopes (Andriamirado *et al* 2021a, Molina *et al* 2021, Almazán *et al* 2022a). This spectral data-model discrepancy appears to be common across all prediction types, even after the introduction of updated fission yield and nuclear structure datasets (Estienne *et al* 2019). The universality of this problem indicates an issue with an input common to both prediction techniques, such as the assumed theoretical shape of the beta spectra used in both calculations (Sonzogni *et al* 2017).

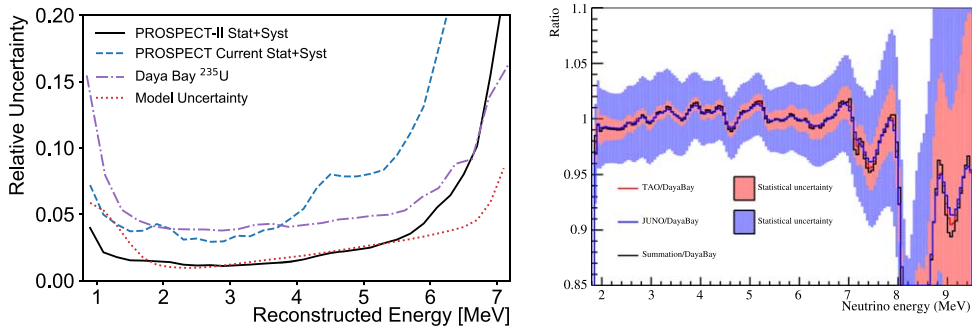


**Figure 14.** Left: PROSPECT-II $^{235}$U spectrum measurement uncertainties after two years of data-taking. From Andriamirado *et al* (2022). Right: comparison of projected JUNO-TAO and JUNO measurements and uncertainties with Daya Bay measurements, assuming that the true LEU reactor spectrum measured by JUNO-TAO and JUNO is given by Estienne *et al* (2019); JUNO-TAO's sensitivity to fine structure in the LEU reactor antineutrino spectrum is clearly illustrated. From Abusleme *et al* (2020).

### *7.4. Future improvements in understanding isotopic neutrino emissions*

A range of ongoing and future experimental IBD-based efforts offer the promise of improving the precision of isotopic antineutrino flux and spectrum measurements. Most recently, the NEOS-II experiment was deployed in Sep, 2018, and has just completed a ∼500 d reactor-on data taking period encompassing the entire fuel cycle of a single 2.8 GW commercial LEU core at the YoungKwang Hanbit nuclear power plant. The experiment aims to measure the IBD rate and energy spectrum of this reactor core at 24 m baseline and perform an analysis of antineutrino spectrum and flux evolution. While its IBD statistics are unlikely to approach those provided by Daya Bay, its single-core measurement enables it to observe a broader range of reactor fuel content, potentially enabling isotopic measurements comparable to Daya Bay and RENO. Plausible gains in isotopic IBD yield measurement precision achievable in a single-core LEU experiment are overviewed in Gebre *et al* (2018).

Beyond this, a pair of proposed future high-precision short-baseline reactor experiments aim to build on recent successes utilizing neutrinos to enhance understanding of nuclear data. The PROSPECT collaboration has proposed a follow-up measurement with an improved detector called PROSPECT-II to be deployed at 7-9 m from the High Flux Isotope Reactor at Oak Ridge National Lab (PROSPECT Collaboration 2020a). The proposed run plan will increase its acquired IBD dataset by more than a factor of five over PROSPECT's first run, alongside an increased signal-to-background ratio. Additionally, PROSPECT plans a new measurement of the absolute flux of neutrinos from $^{235}$U reaching a ∼2.5% precision primarily limited by knowledge of the HFIR reactor core's thermal power. These measurements will provide an important test of theoretical models in a simple system primarily composed of a single fissile isotope, $^{235}$U. The expected $^{235}$U spectrum measurement uncertainties of PROSPECT-II uncertainty are shown in figure 14: its $^{235}$U precision will substantially exceed Daya Bay, and will rival that of the theoretical models. Subsequent deployment of PROSPECT-II at an LEU reactor would allow correlated flux measurements between core types, further enhancing knowledge of individual isotopic contributions, again outlined in Gebre *et al* (2018).

In southern China, a high-resolution ($<2\%/\sqrt{E\ (\mathrm{MeV})}$) satellite detector for the JUNO project, called JUNO-TAO, is in the development phase and will be deployed at ∼25 m from

one LEU reactor at the Taishan nuclear power plant (Abusleme *et al* 2020). JUNO-TAO will collect a large (millions) IBD dataset with excellent energy resolution over multiple fuel cycles, which should enable searches for sub-structure in the neutrino spectrum from individual beta-decays, as shown in figure 14. When analyzed in combination with a high-precision HEU experiment, such as that provided by PROSPECT-II, these datasets should enable major improvements in knowledge of the antineutrino spectrum produced after $^{239}$Pu and $^{238}$U fissions.

Data-model discrepancies have been authoritatively demonstrated by recent high-precision reactor antineutrino measurements. A resolution of this picture will likely require not just improvements in IBD datasets, but also the advancement of a variety of non-IBD nuclear physics and neutrino datasets. An overview of relevant recommendations for improving non-IBD datasets can be found in (Fallot *et al* 2019, Romano *et al* 2022).

On the conversion prediction side, recent Russian measurements of aggregate beta spectrum/yield ratios have cast doubt on the accuracy of the original ILL datasets (Kopeikin *et al* 2021, 2021). To authoritatively resolve this issue, a high-precision aggregate beta spectrum measurement using modern neutron facilities and measurement techniques should be performed for all major and minor fission isotopes. The robustness of both conversion and summation predictions could be enhanced via measurement of beta spectrum shapes for a few forbidden beta decay transitions of high-$Q$ isotopes that provide a dominant contribution to the high-energy reactor antineutrino spectrum. Such a measurement would verify this key theoretical input to both calculations. For summation predictions, continuation of total absorption gamma spectroscopy (TAGS) measurements should be carried out to further minimize the incidence of Pandemonium-affected data in the nuclear data.

Up to this point, direct antineutrino measurements have been unable to test the accuracy of summation modelling below the 1.8 MeV proton IBD interaction threshold. High-precision measurements of recoil spectra from the threshold-free CEvNS interaction at reactors offer the promise of addressing this current weakness in the global antineutrino flux picture.

## 8. Reactor antineutrino detection research and development

### *8.1. Reactor antineutrino detection technologies*

The reactor neutrino sub-field has been particularly prolific within the broader scope of neutrino physics in recent years. However, persistent tensions between the results of multiple short baseline experiments, together with the yet to-be realized detection of CE$\nu$NS using reactor neutrinos, are strong reasons to continue improving on current techniques and developing new enabling technologies. To ensure a broad range for known and unknown physics with reactor neutrinos, it is necessary that new experiments and development efforts cover a wide range of detection principles. In this section, we provide a condensed description of the many current initiatives in pursuit of low-threshold and/or MeV-scale reactor antineutrino detection.

### *8.2. Very low energy detection*

Coherent scattering of neutrinos off nuclei has become a growing field of interest in reactor neutrino physics and neutrino physics in general. For coherent scattering, the neutrino energy transfer occurs with the entire nucleus rather than a single nucleon, meaning that energy transfer has to be very low. In addition, a large fraction of transferred energy is released as heat or lost due to quenching effects. While coherent scattering was already discovered at

high energy spallation neutron sources, fully coherent scattering would happen only at low reactor energies and thus very sensitive new detector technologies are required. These detectors need to offer a low threshold and low noise levels. In addition, those detectors require a thick shielding and overburden as they are running close to a continuous reactor, as opposed to having an accelerator-based timing reference signal to suppress background.

The use of low-threshold detectors for performing novel non-standard physics searches was described previously in sections 5 and 6. Since coherent scattering detectors in reactor neutrino physics are sensitive to very low energies, implemented technologies also offer promise beyond reactor neutrino detection. For example, such a technology would also be useful in probing the scattering of low-mass dark matter. First results have already been delivered on these topics. In the following, different types of low energy detectors in the context of coherent neutrino nucleus scattering are discussed.

P-type High Purity Germanium Detectors. These detectors belong to the class of ionization detectors. Unlike conventional n-type point contact technology, p-type point contact permits high purity Ge detectors to bypass the characteristic limited charge collection efficiency and degraded energy resolution. This results in reduced capacitance while offering a large detector volume of about 1 kg per detector unit. The small value of the capacitance results in low electronic noise and allows to lower the detection threshold to values between 200 and 300 eV electron equivalent ionization energy. A mechanical cooling is commonly used and shielding is either employed via sandwiches of lead, copper, polyethylene or active vetoing through scintillation crystals. There are four major experiments at the commissioning or data-taking stage that could reveal a positive detection of reactor neutrino CE$\nu$NS in the near future: CONUS (Bonet *et al* 2021b), NuGEN (Belov *et al* 2015), TEXONO (Soma *et al* 2016) and the NCC-1701 vessel at Dresden-II nuclear reactor (Colaresi *et al* 2021).

Skipper Si CCD. In the most general sense, the interaction principle of Charge-Coupled Device (CCD) is based on the photoelectric effect, where incident photons are absorbed in a silicon substrate generating as a consequence one or more electron-hole pairs. In conventional scientific CCDs, low-frequency readout noise results in variations in the measured charge per pixel creating a fundamental limitation on precise single-photon counting. Some initiatives like CONNIE (Aguilar-Arevalo *et al* 2016) have been applying CCDs to neutrino detection for many years, providing an upper limit for reactor CE$\nu$NS event rate.

However, in the recent years, a new noise-reduction technique has emerged based in the use of a floating gate output stage to perform repeated charge measurements for each pixel. This multiple readout technique was implemented in the form of a Skipper-CCD achieving ultra-low readout noise that stood several orders of magnitude below values obtained with conventional CCD detection (Tiffenberg *et al* 2017a). The application of this novel technology is expected to bring unprecedented detection precision down to the eV energy scale. CONNIE recently upgraded to Skipper-CCDs (Nasteva 2021) showing preliminary stable and very low values of readout noise. Another new initiative called $\nu$IOLETA has taken the chance to join the efforts for building a kg-scale experiment based on Skipper-CCDs projecting a 90% C.L observation of CE$\nu$NS in 1.5 days of data taking.

Besides allowing high precision measurements of the SM at low energies, Skipper-CCD might enable a unique exploration of any physics hiding beyond that. Light-boson mediated interactions, neutrino magnetic moment or dark matter searches are strong candidates to be investigated.

Noble Element Detectors. Noble element detectors, especially liquid xenon (LXe) and liquid argon (LAr) detectors, have been developed during the last decade mainly for direct dark matter searches. One of their main advantages is the extremely low detection threshold, a feature that makes noble element technology an excellent candidate to observe CE$\nu$NS. By

means of time projection chambers filled with the aforementioned noble elements, low energy interactions like these have been sought by analyzing ionization signals, but to date the sensitivity in the few-electron region has been compromised by backgrounds. The most recognizable effort trying to observe CE$\nu$NS using this technology is the RED collaboration (Akimov *et al* 2017). This experiment uses a dual phase xenon detector of 100kg fiducial volume. Ionization electrons created in the liquid phase are extracted through electric fields and amplified in the gaseous phase. The scintillation light of about 30 photons per electron in the gaseous phase is then detected by photosensors. This experiment has achieved a low background rate down to 4 ionization electrons while operating at the surface level. R&D efforts to reduce the single-and-few electrons background in noble liquid detectors are being pursued in the NUXE program (Ni 2020, Ni *et al* 2021), which plans to use a 30 kg LXe active target to detect reactor neutrino CEvNS events with signals down to single ionization electrons.

Synergies with dark matter searches using similar technologies exist. More concretely, the observation of CE$\nu$NS using noble gases will provide valuable input for a precise signal and background modeling for next-generation LAr and LXe based dark matter experiments. Finally, it could present a new way to monitor the nuclear fuel cycle using neutrinos for nuclear safeguarding applications.

Bolometers. Bolometers are designed as heat detectors and measure phonons created by nuclear recoils. Operating at mK temperatures, these detectors are able to achieve very low thresholds down to 20 eV. Three collaborations, NUCLEUS (Strauss *et al* 2017, Angloher *et al* 2019), Ricochet (Augier *et al* 2021), and MINER (Agnolet *et al* 2017), are following this strategy. NUCLEUS uses $CaWO_4$ and $Al_2O_3$ crystals, while Ricochet and MINER use Ge/Zn and Ge/Si targets, respectively. To ensure a reasonable energy resolution, the detector crystals in use have to be kept small, in the order of 10 g. An exception is MINER with a detector at the order of 1 kg, since they detect charged particles through phonons created by the charged particles in high field regions of the detector. Their detector therefore belongs rather to the class of ionization detectors. Besides MINER, Ricochet can exploit ionization and heat signals. This allows them, from the comparison of these signals, to perform particle identification and therefore background rejection.

Crystal Scintillator Detectors. An alternative form of scintillation-based detectors revolves around crystal scintillators. One of the main advantages of this technology is the high yield of photons produced by scintillator crystals while producing low amounts of background. The crystals are also relatively accessible and permit for the use of large and relatively inexpensive pieces. The NEON collaboration (Choi 2020) uses short 15 kg NaI crystals to improve the light collection efficiency. Crystals are read out by PMTs on both ends. They achieve a 220 eV energy threshold. An active liquid scintillator veto is surrounding the target crystal. Data taking has started from December 2020 which includes 1 month reactor-off period.

Color Center Passive Detectors. Crystal defects have been identified as candidate for the detection of low energy nuclear recoils. Recently, it was proposed to use materials where these defects act as color centers and to use modern microscopic techniques, specifically selective plane illumination microscopy, to image individual radiation induced color centers in bulk volumes (Cogswell *et al* 2021). This technology could provide passive detectors for reactor CEvNS, both for basic science and also nuclear security applications.

### *8.3. IBD detection technology improvements*

Unlike the previously discussed very low energy detection of coherent neutrino nucleus scattering, reactor neutrino detection via IBD is well established. To improve the scalability

and/or background rejection performance of IBD detectors, novel detector media are currently being investigated (Schoppmann 2023). These developments may improve the achievable physics precision of IBD-based detectors and increase their capability or versatility as reactor monitoring instruments.

$^{6}$Li-doped Organic Scintillators. The study of reactor antineutrinos has traditionally pivoted around organic scintillators. Among common requirements like high scintillation light yield and good optical transmission, organic scintillators need to provide excellent particle identification for fast neutrons and neutron captures in order to properly identify IBD interactions. To successfully fulfill these criteria organic scintillator compounds can be mixed with PSD-capabilities in mind and then doped with a neutron-catcher isotope like $^{6}$Li.

Liquid PSD-capable scintillators with $^{6}$Li-doping (LiLS) have already been produced and used in experiments like PROSPECT at the ton-scale (PROSPECT Collaboration 2020b). Besides its PSD-capabilies, LiLS production is easily scalable which permits larger proton-rich targets with long-term stability at standard temperatures. A complementary alternative to LiLS that permits readily transportation and flexibility comes from $^{6}$Li-doped plastic scintillators (LiPS). While historically plastics have been found to exhibit much poorer discrimination properties, in the recent years significant progress has been made in synthesizing stable PSD-capable plastic scintillators (Zaitseva *et al* 2013), even with dissolved $^{6}$Li (Zaitseva *et al* 2012). Some initiatives like the ROADSTR near-field working group (ROADSTR Near-Field Working Group 2020) and SANDD (Li *et al* 2019) are currently developing novel prototypes for readily mobile reactor antineutrino detectors using PSD-capable LiPS.

Water-based Liquid Scintillators. Monolithic optical detectors have a long history of success in neutrino physics via IBD or ES, from water Cherenkov detectors to liquid scintillator detectors. As new experiments push current limits into previously unexplored regions of phase space, it becomes a priority to develop advanced detection techniques for particle identification and background rejection. A promising new approach is given by exploiting Cherenkov and scintillation signals simultaneously using water-based organic liquid scintillators, i.e water is loaded with $\sim$10 % liquid scintillator (Yeh *et al* 2011, Caravaca *et al* 2020). This technology is foreseen in the Eos experiment and could be deployed in planned experiments for reactor monitoring like AIT-NEO (Askins *et al* 2015). There are also potential synergies with future kilo-ton experiments like Theia (Askins *et al* 2020) which will have a rich physics program including topics in high-energy, nuclear, geo, and astrophysics such as neutrino mass ordering, CP-violation in the leptonic sector, solar neutrinos, diffuse supernova neutrinos, neutrinos from supernova bursts, neutrinos from the Earth's crust, nucleon decay, and neutrinoless double beta decay with sensitivity towards normal neutrino mass ordering.

Powerful aspects are the particle identification (PID) capabilities offered from the Cherenkov/scintillation ratio (Caravaca *et al* 2017). This PID has the potential to significantly improve signal/background discrimination of alpha/beta and beta/gamma particles and arises from two sources: the time profile of scintillation light emitted in response to a recoiling proton may differ from electron-like events due to quenching effects and the ratio of Cherenkov to scintillation light will differ between heavier and lighter particles. Additionally, recent developments have demonstrated the capability to identify neutron/gamma particles through the pulse shape discrimination of the scintillation light (?).

Mixed and Slow Liquid Scintillators. Alternative approaches to improve discrimination power via the time profile of scintillation light exist. This can be achieved by using compound scintillators blended from two or more scintillator components. In addition, varying the concentration of fluors allows to slow down the scintillation pulse time profile. This allows in

particular to distinguish between nuclear and electronic recoils. The recoil protons excite more triplet states of the solvent molecules than electrons or positrons, therefore leading to a different magnitude of quenching. These triplet states have longer decay times increasing the charge ratio in the tail of the scintillation pulse. Blended scintillators were successfully exploited for PID in the past (Kim *et al* 2015, Buck *et al* 2019).

Opaque Scintillator. LiquidO is a detection approach relying on opaque scintillators that represents a departure from conventional scintillation detectors. The main principle resides in stochastically confining light around the production point by reducing the scattering length of photons to below the cm level, while keeping the absorption length high enough to ensure a good light output (Cabrera *et al* 2021). The localised detection of trapped photons provides imaging of topological energy depositions that translates into superior event-by-event identification and position reconstruction. In order to capture the confined light, the detector is traversed by a tight array of optical wave-shifting fibers that collect the light at the interaction point and transport it to photodetectors, typically SiPMs, located at the end of each fiber. While LiquidO can have multiple fiber orientations running simultaneously to reach 3D imaging, it is possible to use timing, if the resolution is good enough, to infer the projected position along the fiber. The LiquidO detection technique is not limited to the use of scintillation. In fact, Cherenkov light can and has been detected this way. However, the use of scintillation is key for low energy neutrino detection. In addition to its imaging capabilities, the opaque medium of LiquidO offers unique opportunities for heavy loading (in the order of 10% or more), as the lack of a transparency requirement relaxes the constraints on the optical model.

An experimental proof-of-concept was successfully run in 2018, called Micro-LiquidO, with an active volume of 0.2 l. Its successor, called Mini-LiquidO, is currently in operation and completing data taking with a volume of 7.5 l. The first opaque scintillating medium used in both LiquidO detectors was NoWaSH (Buck *et al* 2019), an admixture from LAB and PPO as the scintillator and paraffin wax to provide the opacity. This compound has displayed below-cm scattering lengths while keeping a high profile of photons per MeV. Above 40°C it mixes homogeneously with ease, while becoming highly viscous when cooling to room temperature. Preliminary studies of NoWaSH also support the possibility of metal loading into the admixture, a feature much needed for different physics goals. Other solutions for possible opaque scintillators exist (Wagner *et al* 2018) and are in the early stages of R&D within the LiquidO scientific consortium.

In the context of reactor antineutrino IBD detection, LiquidO could have the ability to separate positrons from electrons and gammas on an event-by-event basis, enabling a major improvement of the signal-to-background ratio and reducing the reliance on overburden. LiquidO's native muon-tracking capability with sub-cm precision is also expected to enable a tight control of cosmogenically produced backgrounds. A full 5 ton reactor neutrino program detector has been funded by the EIC-Pathfinder-2021 European program and will start construction in 2024. LiquidO technology is also actively being considered for the detection of solar neutrinos using indium, geoneutrinos, accelerator neutrinos, and double beta decay (Cabrera *et al* 2021, 2023).

Gd-doped Water Gadolinium-doping has long been recognized as a key advance in the context of enhancing sensitivity to neutrons and thus antineutrinos in IBD detectors. The Super-Kamiokande gadolinium upgrade (Abe *et al* 2022) reflects the importance of this technological enhancement for fundamental neutrino physics at the MeV scale. Similarly, Gd-doping presents the opportunity to improve sensitivity to reactors in large-scale detectors, especially for mid-to-far-field monitoring and exclusion applications. Detectors such as the proposed kiloton-scale AIT-NEO detector (Askins *et al* 2015) will permit exploration of

further enhancements to the sensitivity of gadolinum-doped water detectors in both domains. For example the use of smaller and/or faster photosensors offers the prospect of improved vertex resolution compared to SK-Gd, with beneficial effects on fiducialiization and background rejection. The scale of the detector also permits detailed experimental validation of the performance of technologies such as wavelength shifting plates, and new methods for *in situ* characterization of water attenuation in doped media. Reconstruction of supernova directionality through the electron scatter channel may be achievable by tagging IBD events using the gadolinium dopant. AIT-NEO can also be used to study the combined benefits of the essential gadolinium dopant with those coming from alternative media such as water-based liquid scintillator.

### *8.4. Synergies*

The technology overlap between reactor neutrinos and other rare event detection fields like dark matter or neutrinoless double-beta decay allow for interesting synergies that could be exploited.

(a) High Purity Ge detectors: low threshold detection allows for $0\nu\beta\beta$ decay, gamma and x-ray spectroscopy.
(b) Plastic Scintillators: their flexibility could be practical for reactor monitoring purposes through readily mobile neutrino detectors (Bernstein *et al* 2020).
(c) Skipper CCD: nuclear spectroscopy, massive multiplexed optical/near-infrared cosmic surveys to study the dark sector, direct DM searches.
(d) Bolometers: their sensitivity to nuclear recoil make them ideal for dark matter/axion searches or probing the structure of nuclei.
(e) Noble liquids: accurate signal and background modeling for the next generation of dark matter experiments.
(f) Water-based scintillators: strong PID capabilities and broad energy range would allow multi-disciplinary research, including BSM physics like $0\nu\beta\beta$ decay or proton decay.
(g) Opaque scintillators: background suppression and flexible doping allow for multiple types of neutrino research, like $0\nu\beta\beta$ or solar neutrinos.

## 9. Conclusions

As described throughout this paper, nuclear reactors have played a central role in the evolution of neutrino physics over the last seven decades due to their copious electron antineutrino emissions. Advances in detectors and our ability to predict reactor neutrino emissions have lead to discoveries and increasingly precise measurements of neutrino properties. This will continue through the next decade, as planned experiments using Inverse Beta Decay to measure neutrino oscillation parameters at long baselines and search for additional neutrino states at short baselines are constructed. Knowledge of reactor antineutrino fluxes will continue to be refined through direct measurement and calculations based on every improving nuclear reaction databases. This in turn will support a new generation of searches for physics Beyond the Standard Model, e.g. using the CEvNS reaction.

## Acknowledgments

The authors gratefully acknowledge support from the U.S. Department of Energy Office of Science, the U.S. National Science Foundation, the Lawrence Livermore National Laboratory LDRD program, and their respective institutions.

## Data availability statement

No new data were created or analysed in this study.

## ORCID iDs

O A Akindele https://orcid.org/0000-0003-4802-5680
N S Bowden https://orcid.org/0000-0002-6115-0956
C Roca https://orcid.org/0000-0003-4994-5024
J Xu https://orcid.org/000-0001-8084-5609
X Zhang https://orcid.org/0000-0003-2518-3651
R Carr https://orcid.org/0000-0002-4181-5092
A J Conant https://orcid.org/0000-0001-7766-4321
G Fernandez-Moroni https://orcid.org/0000-0003-4238-6813
P Huber https://orcid.org/0000-0002-2622-3953
J M Link https://orcid.org/0000-0002-1514-0650
T J Langford https://orcid.org/0000-0001-5953-5294
B R Littlejohn https://orcid.org/0000-0002-6912-9684
J P Ochoa-Ricoux https://orcid.org/0000-0001-7376-5555
L Strigari https://orcid.org/0000-0001-5672-6079
S Schoppmann https://orcid.org/0000-0002-7208-0578
C Zhang https://orcid.org/0000-0003-2298-6272

## References

Aartsen M G *et al* (IceCube) 2017 PINGU: a vision for neutrino and particle physics at the south pole *J. Phys.* G **44** 054006
Aartsen M G *et al* (IceCube-Gen2) 2020 Combined sensitivity to the neutrino mass ordering with JUNO, the IceCube upgrade, and PINGU *Phys. Rev.* D **101** 032006
Abdelhameed A H *et al* (CRESST Collaboration) 2019 First results from the cresst-iii low-mass dark matter program *Phys. Rev.* D **100** 102002
Abdurashitov J N *et al* (SAGE) 1999 Measurement of the response of the russian-american gallium experiment to neutrinos from a $^{51}$Cr source *Phys. Rev.* C **59** 2246–63
Abdurashitov J N *et al* 2006 Measurement of the response of a Ga solar neutrino experiment to neutrinos from an $^{37}$Ar source *Phys. Rev.* C **73** 045805
Abe S *et al* (KamLAND) 2008 Precision measurement of neutrino oscillation parameters with KamLAND *Phys. Rev. Lett.* **100** 221803
Abe K *et al* (T2K) 2011 Indication of electron neutrino appearance from an accelerator-produced off-axis muon neutrino beam *Phys. Rev. Lett.* **107** 041801
Abe Y *et al* (Double Chooz) 2012 Indication of reactor $\bar{\nu}_e$ disappearance in the double chooz experiment *Phys. Rev. Lett.* **108** 131801
Abe Y *et al* (Double Chooz) 2012a First test of lorentz violation with a reactor-based antineutrino experiment *Phys. Rev.* D **86** 112009
Abe Y *et al* (Double Chooz) 2012b Reactor electron antineutrino disappearance in the double chooz experiment *Phys. Rev.* D **86** 052008

Abe Y *et al* (Double Chooz) 2014 Improved measurements of the neutrino mixing angle $\theta_{13}$ with the double chooz detector *J. High Energy Phys.* JHEP10(2014)086
Abe K *et al* (T2K) 2015 Search for short baseline $\nu_e$ disappearance with the T2K near detector *Phys. Rev.* D **91** 051102
Abe K *et al* (Hyper-Kamiokande) 2018 Hyper-kamiokande design report arXiv:1805.04163
Abe K *et al* (T2K) 2021 Improved constraints on neutrino mixing from the T2K experiment with $3.13 \times 10^{21}$ protons on target *Phys. Rev.* D **103** 112008
Abe K *et al* (Super-Kamiokande) 2022 First gadolinium loading to super-kamiokande *Nucl. Instrum. Meth.* A **1027** 166248
Abi B *et al* (DUNE) 2020 Deep underground neutrino experiment (DUNE), far detector technical design report, volume II: DUNE physics arXiv:2002.03005
Abi B *et al* (DUNE) 2020a Long-baseline neutrino oscillation physics potential of the DUNE experiment *Eur. Phys. J.* C **80** 978
Abi B *et al* (DUNE) 2021 Supernova neutrino burst detection with the deep underground neutrino experiment *Eur. Phys. J.* C **81** 423
Abrahão T *et al* (Double Chooz) 2021a Search for signatures of sterile neutrinos with double chooz *Eur. Phys. J.* C **81** 775
Abrahão T *et al* (Double Chooz) 2021 Reactor rate modulation oscillation analysis with two detectors in double chooz *J. High Energy Phys.* JHEP01(2021b)190
Abratenko P *et al* (MicroBooNE) 2022 Search for an excess of electron neutrino interactions in MicroBooNE using multiple final-state topologies *Phys. Rev. Lett.* **128** 241801
Abreu Y *et al* (SoLid) 2017 A novel segmented-scintillator antineutrino detector *J. Instrum.* **12** P04024
Abud Abed A *et al* (DUNE) 2022 Low exposure long-baseline neutrino oscillation sensitivity of the DUNE experiment *Phys. Rev.* D **105** 072006
Abusleme A *et al* (JUNO) 2020 TAO conceptual design report: a precision measurement of the reactor antineutrino spectrum with sub-percent energy resolution arXiv:2005.08745
Abusleme A *et al* (JUNO) 2021 Calibration strategy of the JUNO experiment *J. High Energy Phys.* **03** 004
Abusleme A *et al* (JUNO) 2022a JUNO physics and detector *Prog. Part. Nucl. Phys.* **123** 103927
Abusleme A *et al* (JUNO) 2022b Sub-percent precision measurement of neutrino oscillation parameters with JUNO *Chin. Phys.* C **46** 123001
Acero M A *et al* (NOvA) 2022 Improved measurement of neutrino oscillation parameters by the NOvA experiment *Phys. Rev.* D **106** 032004
Acero M A, Giunti C and Laveder M 2008 Limits on $\nu_e$ and $\overline{\nu}_e$ disappearance from gallium and reactor experiments *Phys. Rev.* D **78** 073009
Achkar B *et al* 1996 Comparison of anti-neutrino reactor spectrum models with the Bugey-3 measurements *Phys. Lett.* B **374** 243–8
Adam B, Bowden N, Goldblum B L, Huber P, Jovanovic I and Mattingly J 2020 Colloquium: neutrino detectors as tools for nuclear security *Rev. Mod. Phys.* **92** 011003
Adams M, Bezrukov F, Elvin-Poole J, Evans J J, Guzowski P, Fearraigh B Ó and Söldner-Rembold S 2020 Direct comparison of sterile neutrino constraints from cosmological data, $\nu_e$ disappearance data and $\nu_\mu \to \nu_e$ appearance data in a 3+1 model *Eur. Phys. J.* C **80** 758
Adamson P *et al* (MINOS) 2011 Improved search for muon-neutrino to electron-neutrino oscillations in MINOS *Phys. Rev. Lett.* **107** 181802
Adamson P *et al* (MINOS+) 2020a Precision constraints for three-flavor neutrino oscillations from the full MINOS+ and MINOS dataset *Phys. Rev. Lett.* **125** 131802
Adamson P *et al* (MINOS+, Daya Bay) 2020b Improved constraints on sterile neutrino mixing from disappearance searches in the MINOS, MINOS+, daya bay, and bugey-3 experiments *Phys. Rev. Lett.* **125** 071801
Adey D *et al* (Daya Bay) 1958 Measurement of the electron antineutrino oscillation with 1958 days of operation at daya bay *Phys. Rev. Lett.* **121** 24180 5
Adey D *et al* (Daya Bay) 2018 Search for a time-varying electron antineutrino signal at daya bay *Phys. Rev.* D **98** 092013
Adey D *et al* (Daya Bay) 2019a Improved measurement of the reactor antineutrino flux at daya bay *Phys. Rev.* D **100** 052004
Adey D *et al* (Daya Bay) 2019b *Phys. Rev. Lett.* **123** 111801
Adrian-Martinez S *et al* (KM3Net) 2016 Letter of intent for KM3NeT 2.0 *J. Phys.* G **43** 084001

Agnes P *et al* (DarkSide Collaboration) 2018 Low-mass dark matter search with the darkside-50 experiment *Phys. Rev. Lett.* **121** 081307
Agnes P *et al* (DarkSide Collaboration) 2021 Calibration of the liquid argon ionization response to low energy electronic and nuclear recoils with darkside-50 *Phys. Rev.* D **104** 082005
Agnolet G *et al* (MINER) 2017 Background studies for the MINER coherent neutrino scattering reactor experiment *Nucl. Instrum. Meth.* A **853** 53–60
Agostini M and Neumair B 2020 Statistical methods applied to the search of sterile neutrinos *Eur. Phys. J.* C **80** 750
Aguilar A *et al* (LSND Collaboration) 2001 Evidence for neutrino oscillations from the observation of $\overline{\nu}_e$ appearance in a $\overline{\nu}_\mu$ beam *Phys. Rev.* D **64** 112007
Aguilar-Arevalo A A *et al* (MiniBooNE) 2013 Improved search for $\nu_\mu \to \bar{\nu}_e$ oscillations in the MiniBooNE experiment *Phys. Rev. Lett.* **110** 161801
Aguilar-Arevalo A *et al* 2016 The connie experiment *J. Phys. Conf. Ser.* **761** 012057
Aguilar-Arevalo A *et al* (MiniBooNE Collaboration) 2018 Significant excess of electronlike events in the MiniBooNE short-baseline neutrino experiment *Phys. Rev. Lett.* **121** 221801
Aguilar-Arevalo A *et al* (CONNIE) 2019 Exploring low-energy neutrino physics with the coherent neutrino nucleus interaction experiment *Phys. Rev.* D **100** 092005
Aguilar-Arevalo A *et al* (CONNIE) 2020 Search for light mediators in the low-energy data of the CONNIE reactor neutrino experiment *J. High Energy Phys.* JHEP04(2020a)054
Aguilar-Arevalo A *et al* (DAMIC Collaboration) 2020b Results on low-mass weakly interacting massive particles from an 11 kg d target exposure of damic at snolab *Phys. Rev. Lett.* **125** 241803
Aguilar-Arevalo A A *et al* (MiniBooNE) 2021 Updated MiniBooNE neutrino oscillation results with increased data and new background studies *Phys. Rev.* D **103** 052002
Aguilar-Arevalo A *et al* (CONNIE) 2022 Search for coherent elastic neutrino-nucleus scattering at a nuclear reactor with CONNIE 2019 data *J. High Energy Phys.* JHEP05(2022)017
Ahmad Q R *et al* (SNO) 2002 Direct evidence for neutrino flavor transformation from neutral current interactions in the sudbury neutrino observatory *Phys. Rev. Lett.* **89** 011301
Ahn J *et al* (RENO Collaboration) 2012 *Phys. Rev. Lett.* **108** 191802
Aker M *et al* (KATRIN) 2021 Bound on 3+1 active-sterile neutrino mixing from the first four-week science Run of KATRIN *Phys. Rev. Lett.* **126** 091803
Aker M *et al* (KATRIN) 2022 Improved eV-scale sterile-neutrino constraints from the second KATRIN measurement campaign *Phys. Rev.* D **105** 072004
Akerib D S *et al* 2020 Investigation of background electron emission in the lux detector *Phys. Rev.* D **102** 092004
Akerib D S *et al* (LUX Collaboration) 2021 Improving sensitivity to low-mass dark matter in lux using a novel electrode background mitigation technique *Phys. Rev.* D **104** 012011
Akimov D *et al* 2017 Status of the RED-100 experiment *J. Instrum.* **12** C06018C06018–06018
Akindele O *et al* 2021 Nu tools: exploring practical roles for neutrinos in nuclear energy and security arXiv:2112.12593
Akindele O A and Zhang X 2020 Mutual benefits derived from the application of neutrino physics to nuclear energy & safeguards Snowmass 2021 Letter of Interest
Alarcon J M, Martin Camalich J and Oller J A 2012 The chiral representation of the $\pi N$ scattering amplitude and the pion-nucleon sigma term *Phys. Rev.* D **85** 051503
Alarcon J M, Geng L S, Martin Camalich J and Oller J A 2014 The strangeness content of the nucleon from effective field theory and phenomenology *Phys. Lett.* B **730** 342–6
Albanese V *et al* (SNO+) 2021 The SNO+ experiment *J. Instrum.* **16** P08059
Alekseev I *et al* (DANSS) 2018 Search for sterile neutrinos at the DANSS experiment *Phys. Lett.* B **787** 56–63
Algora A *et al* 2010 Reactor decay heat in $^{239}$Pu: solving the $\gamma$ discrepancy in the 4–3000 s cooling period *Phys. Rev. Lett.* **105** 202501
Almazán H *et al* (STEREO) 2018 Sterile neutrino constraints from the STEREO experiment with 66 days of reactor-on data *Phys. Rev. Lett.* **121** 161801
Almazán H *et al* (STEREO) 2020a Accurate measurement of the electron antineutrino yield of $^{235}$U fissions from the STEREO experiment with 119 days of reactor-on data *Phys. Rev. Lett.* **125** 201801
Almazán H *et al* (STEREO) 2020b Improved sterile neutrino constraints from the STEREO experiment with 179 days of reactor-on data *Phys. Rev.* D **102** 052002
Almazán H *et al* (Stereo, Prospect) 2022a Joint measurement of the $^{235}$U antineutrino spectrum by prospect and stereo *Phys. Rev. Lett.* **128** 081802

Almazán H *et al* 2022b Searching for hidden neutrons with a reactor neutrino experiment: constraints from the STEREO experiment *Phys. Rev. Lett.* **128** 061801
Amaral D W *et al* 2020 Constraints on low-mass, relic dark matter candidates from a surface-operated supercdms single-charge sensitive detector *Phys. Rev.* D **102** 091101
An F P *et al* (Daya Bay) 2012 Observation of electron-antineutrino disappearance at daya bay *Phys. Rev. Lett.* **108** 171803
An F P *et al* (Daya Bay) 2014 Spectral measurement of electron antineutrino oscillation amplitude and frequency at daya bay *Phys. Rev. Lett.* **112** 061801
An F *et al* (JUNO) 2016a Neutrino physics with JUNO *J. Phys.* G **43** 030401
An F P *et al* (Daya Bay) 2016b The detector system of the daya bay reactor neutrino experiment *Nucl. Instrum. Meth.* A **811** 133–61
An F P *et al* (Daya Bay) 2016d Improved search for a light sterile neutrino with the full configuration of the daya bay experiment *Phys. Rev. Lett.* **117** 151802
An F P *et al* (Daya Bay) 2017a Study of the wave packet treatment of neutrino oscillation at daya bay *Eur. Phys. J.* C **77** 606
An F P *et al* (Daya Bay) 2017b Improved measurement of the reactor antineutrino flux and spectrum at daya bay *Chin. Phys.* C **41** 013002
An F P *et al* (Daya Bay) 2017c Evolution of the reactor antineutrino flux and spectrum at daya bay *Phys. Rev. Lett.* **118** 251801
An F P *et al* (Daya Bay) 2021 Antineutrino energy spectrum unfolding based on the daya bay measurement and its applications *Chin. Phys.* C **45** 073001
An F P *et al* (Daya Bay, PROSPECT) 2022 Joint determination of reactor antineutrino spectra from $^{235}$U and $^{239}$Pu fission by daya bay and prospect *Phys. Rev. Lett.* **128** 081801
Andriamirado M *et al* (PROSPECT, STEREO) 2020 Preparation of the Neutrino-4 experiment on search for sterile neutrino and the obtained results of measurements arXiv:2006.13147
Andriamirado M *et al* (PROSPECT) 2021a Improved short-baseline neutrino oscillation search and energy spectrum measurement with the PROSPECT experiment at HFIR *Phys. Rev.* D **103** 032001
Andriamirado M *et al* (PROSPECT, PROSPECT Collaboration)∗ 2021b Limits on sub-GeV dark matter from the PROSPECT reactor antineutrino experiment *Phys. Rev.* D **104** 012009
Andriamirado M *et al* (PROSPECT) 2022 PROSPECT-II physics opportunities *J. Phys.* G **49** 070501
Angloher G *et al* (NUCLEUS) 2019 Exploring CE$\nu$NS with NUCLEUS at the chooz nuclear power plant *Eur. Phys. J.* C **79** 1018
Antonello M *et al* (MicroBooNE, LAr1-ND, ICARUS-WA104) 2015 A Proposal for a Three Detector Short-Baseline Neutrino Oscillation Program in the Fermilab Booster Neutrino Beam arXiv:1503.01520
Apollonio M *et al* (CHOOZ) 1999 Limits on neutrino oscillations from the CHOOZ experiment *Phys. Lett.* **466** 415–30
Aprile E *et al* (XENON Collaboration) 2019 Light dark matter search with ionization signals in xenon1t *Phys. Rev. Lett.* **123** 251801
Araki T *et al* (KamLAND) 2005 Measurement of neutrino oscillation with KamLAND: evidence of spectral distortion *Phys. Rev. Lett.* **94** 081801
Archidiacono M, Fornengo N, Giunti C, Hannestad S and Melchiorri A 2013 Sterile neutrinos: cosmology versus short-baseline experiments *Phys. Rev.* D **87** 125034
Argüelles C A, Bertólez-Martínez T and Salvado J 2023 Impact of wave packet separation in low-energy sterile neutrino searches *Phys. Rev.* D **107** 036004
Argüelles C A, Esteban I, Hostert M, Kelly K J, Kevin J, Kopp J, Machado P A N, Martinez-Soler I and Perez-Gonzalez Y F 2022 MicroBooNE and the $\nu$e interpretation of the MiniBooNE low-energy excess *Phys. Rev. Lett.* **128** 241802
Aristizabal S D, Romeri V D, Flores L J and Papoulias D K 2021 Axionlike particles searches in reactor experiments *J. High Energy Phys.* **2021** 294
Armbruster B *et al* 1998 KARMEN limits on $\nu_e \rightarrow \nu_\tau$ oscillations in $2-\nu$ and $3-\nu$ mixing schemes *Phys. Rev.* C **57** 3414–24
Ashenfelter J *et al* (PROSPECT) 2018 First search for short-baseline neutrino oscillations at HFIR with PROSPECT *Phys. Rev. Lett.* **121** 251802
Ashenfelter J *et al* (PROSPECT) 2019 Measurement of the antineutrino spectrum from $^{235}$U fission at HFIR with PROSPECT *Phys. Rev. Lett.* **122** 251801
Askins M *et al* (WATCHMAN) 2015 The physics and nuclear nonproliferation goals of WATCHMAN: a WAter CHerenkov monitor for ANtineutrinos arXiv:1502.01132

Askins M *et al* (Theia) 2020 THEIA: an advanced optical neutrino detector *Eur. Phys. J.* C **80** 416
Auerbach L B *et al* (LSND) 2001 Measurements of charged current reactions of $\nu_e$ on $^{12}$C *Phys. Rev.* C **64** 065501
Augier C *et al* (Ricochet) 2021 Ricochet progress and status *19th Int. Workshop on Low Temperature Detectors*
Back A R *et al* (ANNIE) 2017 Accelerator neutrino neutron interaction experiment (ANNIE): preliminary results and physics phase proposal arXiv:1707.08222
Bai Y and Berger J 2020 Nucleus capture by macroscopic dark matter *J. High Energy Phys.* JHEP05 (2020)160
Bak G *et al* (RENO) 2018 Measurement of reactor antineutrino oscillation amplitude and frequency at RENO *Phys. Rev. Lett.* **121** 201801
Bak G *et al* (RENO) 2019 Fuel-composition dependent reactor antineutrino yield at RENO *Phys. Rev. Lett.* **122** 232501
Barak L *et al* (SENSEI Collaboration) 2020 Sensei: direct-detection results on sub-gev dark matter from a new skipper ccd *Phys. Rev. Lett.* **125** 171802
Barinov V V *et al* 2022a Results from the baksan experiment on sterile transitions (BEST) *Phys. Rev. Lett.* **128** 232501
Barinov V V *et al* 2022b A search for electron neutrino transitions to sterile states in the BEST experiment arXiv:2201.07364
Barinov V and Gorbunov D 2021 BEST impact on sterile neutrino hypothesis arXiv:2109.14654
Bass M *et al* 2015 Baseline optimization for the measurement of CP violation, mass hierarchy, and $\theta_{23}$ octant in a long-baseline neutrino oscillation experiment *Phys. Rev.* D **91** 052015
Basto-Gonzalez V S, Forero D V, Giunti C, Quiroga A A and Ternes C A 2022 Short-baseline oscillation scenarios at JUNO and TAO *Phys. Rev.* D **105** 075023
Batell B, Pospelov M and Ritz A 2009 Exploring portals to a hidden sector through fixed targets *Phys. Rev.* D **80** 095024
Behera S P, Mishra D K and Pant L M 2020 Active-sterile neutrino mixing constraints using reactor antineutrinos with the ISMRAN setup *Phys. Rev.* D **102** 013002
Belov V *et al* 2015 The nugen experiment at the kalinin nuclear power plant *J. Instrum.* **10** P12011–12011
Bernstein A, Bowden N S and Erickson A S 2018 Reactors as a source of antineutrinos: the effect of fuel loading and burnup for mixed oxide fuels *Phys. Rev. Applied* **9** 014003
Berryman J M 2019 Constraining sterile neutrino cosmology with terrestrial oscillation experiments *Phys. Rev.* D **100** 023540
Berryman J M and Huber P 2020 Reevaluating reactor antineutrino anomalies with updated flux predictions *Phys. Rev.* D **101** 015008
Berryman J M and Huber P 2021 Sterile neutrinos and the global reactor antineutrino dataset *J. High Energy Phys.* JHEP01(2021)167
Berryman J M, Coloma P, Huber P, Schwetz T and Zhou A 2022 Statistical significance of the sterile-neutrino hypothesis in the context of reactor and gallium data *J. High Energy Phys.* JHEP02 (2022)055
Bhupal Dev P S *et al* 2019 Neutrino non-standard interactions: a status report 001 arXiv:1907.00991
Billard J *et al* 2017 Coherent neutrino scattering with low temperature bolometers at chooz reactor complex *J. Phys.* G **44** 105101
Boehm F *et al* 2001 Final results from the palo verde neutrino oscillation experiment *Phys. Rev.* D **64** 112001
Boireau G *et al* (NUCIFER) 2016 Online monitoring of the osiris reactor with the nucifer neutrino detector *Phys. Rev.* D **93** 112006
Bonet H *et al* (CONUS) 2021a Constraints on elastic neutrino nucleus scattering in the fully coherent regime from the CONUS experiment *Phys. Rev. Lett.* **126** 041804
Bonet H *et al* 2021b Large-size sub-keV sensitive germanium detectors for the CONUS experiment *Eur. Phys. J.* C **81** 267
Bonhomme A *et al* 2022 Direct measurement of the ionization quenching factor of nuclear recoils in germanium in the keV energy range *Eur. Phys. J.* C **82** 815
Bramante J, Broerman B, Lang R F and Raj N 2018 Saturated overburden scattering and the multiscatter frontier: discovering dark matter at the planck mass and beyond *Phys. Rev.* D **98** 083516
Bramante J, Broerman B, Kumar J, Lang R F, Pospelov M and Raj N 2019 Foraging for dark matter in large volume liquid scintillator neutrino detectors with multiscatter events *Phys. Rev.* D **99** 083010

Bridle S, Elvin-Poole J, Evans J, Fernandez S, Guzowski P and Soldner-Rembold S 2017 A combined view of sterile-neutrino constraints from CMB and neutrino oscillation measurements *Phys. Lett.* B **764** 322–7
Buck C, Gramlich B and Schoppmann S 2019 Novel opaque scintillator for neutrino detection *J. Instrum.* **14** P11007P11007–11007
Cabrera A *et al* 2021 Neutrino physics with an opaque detector *Commun. Phys.* **4** 273
Cabrera A *et al* 2022 Synergies and prospects for early resolution of the neutrino mass ordering *Sci. Rep.* **12** 5393
Cabrera A *et al* (LiquidO Consortium) 2023 Probing earth's missing potassium using the unique antimatter signature of geoneutrinos arXiv:2308.04154
Cao G, Ochoa-Ricoux J P, Wang W, Wen L, Wurm M and Zhan L 2020 The JUNO-TAO experiment *Snowmass 2021 Letter of Interest*
Capozzi F, Li S W, Zhu G and Beacom J F 2019 DUNE as the next-generation solar neutrino experiment *Phys. Rev. Lett.* **123** 131803
Cappiello C and Beacom J F 2019 Strong new limits on light dark matter from neutrino experiments *Phys. Rev.* **D100** 103011
Caravaca J, Land B J, Yeh M and Orebi Gann G D 2020 Characterization of water-based liquid scintillator for cherenkov and scintillation separation *Eur. Phys. J.* C **80** 867
Caravaca J, Descamps F B, Land B J, Yeh M and Orebi Gann G D 2017 Cherenkov and scintillation light separation in organic liquid scintillators *Eur. Phys. J.* C **77** 811
Carroll J *et al* 2018 Monitoring reactor anti-neutrinos using a plastic scintillator detector in a mobile laboratory arXiv:1811.01006
Cerdeno D G, Fairbairn M, Jubb T, Machado P A N, Vincent A C and hm C B 2016 Physics from solar neutrinos in dark matter direct detection experiments *J. High Energy Phys.* JHEP05(2016)118
Chau N, Athayde Marcondes de André J P, Van Elewyck V, Kouchner A, Kalousis L, Dracos M *et al* (KM3NeT, JUNO) 2021 Neutrino mass ordering determination through combined analysis with JUNO and KM3NeT/ORCA *J. Instrum.*C **16** 11007
Chavarria A E 2016 Measurement of the ionization produced by sub-kev silicon nuclear recoils in a ccd dark matter detector *Phys. Rev.* D **94** 082007
PROSPECT Collaboration 2020b Forthcoming science from the PROSPECT-I data set *Snowmass 2021 Letter of Interest*
Choi J H *et al* (RENO) 2016 Observation of energy and baseline dependent reactor antineutrino disappearance in the RENO experiment *Phys. Rev. Lett.* **116** 211801
Choi J J 2020 Neutrino elastic-scattering observation with NaI[Tl](NEON) *PoS* **NuFact2019** 047
Choi J H *et al* (RENO) 2020a Search for Sub-eV sterile neutrinos at RENO *Phys. Rev. Lett.* **125** 191801
Choi J J *et al* 2020b Improving the light collection using a new NaI(Tl) crystal encapsulation *Nucl. Instrum. Meth.* A **981** 164556
Christian B, Gramlich B, Lindner M, Roca C and Schoppmann S 2019 Production and properties of the liquid scintillators used in the stereo reactor neutrino experiment *J. Instrum.* **14** P01027
Cirelli M, Nobile E D and Panci P 2013 Tools for model-independent bounds in direct dark matter searches *J. Cosmol. Astropart. Phys.* JCAP10(2013)019
Cogswell B K, Goel A and Huber P 2021 Passive low-energy nuclear-recoil detection with color centers *Phys. Rev. Appl.* **16** 064060
Colaresi J, Collar J I, Hossbach T W, Kavner A R L, Lewis C M, Robinson A E and Yocum K M 2021 First results from a search for coherent elastic neutrino-nucleus scattering at a reactor site *Phys. Rev.* D **104** 072003
Coloma P, Huber P and Schwetz T 2021 Statistical interpretation of sterile neutrino oscillation searches at reactors *Eur. Phys. J.* C **81** 2
Conant A J and Surukuchi P T 2020 Prediction and measurement of the reactor neutrino flux and spectrum *Snowmass 2021 Letter of Interest*
Conrad J M and Shaevitz M H 2012 Limits on electron neutrino disappearance from the KARMEN and LSND $\nu_e$-carbon cross section data *Phys. Rev.* D **85** 013017
Conrad J M, Ignarra C M, Karagiorgi G, Shaevitz M H and Spitz J 2013 Sterile neutrino fits to short baseline neutrino oscillation measurements *Adv. High Energy Phys.* **2013** 163897
Danilov M 2021 New results from the danss experiment *Presented at EPS-HEP 2021 Virtual Conf.* https://indico.desy.de/event/28202/contributions/105957/
Danilov M, Demidov S and Gorbunov D 2019 Constraints on hidden photons produced in nuclear reactors *Phys. Rev. Lett.* **122** 041801

Davis R, Harmer D and Hoffman K 1968 *Phys. Rev. Lett.* **20** 1205
de Gouvea A, de Romeri V and Ternes C A 2020 Probing neutrino quantum decoherence at reactor experiments *J. High Energy Phys.* JHEP08(2020)018
de Gouvêa A and Kelly K J 2016 False signals of CP-invariance violation at DUNE arXiv:1605.09376
de Gouvêa A, Kelly K J and Kobach A 2015 CP-invariance violation at short-baseline experiments in 3 +1 neutrino scenarios *Phys. Rev.* D **91** 053005
de Gouvêa A, Romeri V D and Ternes C A 2021 Combined analysis of neutrino decoherence at reactor experiments *J. High Energy Phys.* JHEP06(2021)042
de Gouvêa A, Peres O L G, Prakash S and Stenico G V 2020 On the decaying-sterile neutrino solution to the electron (anti)neutrino appearance anomalies *J. High Energy Phys.* JHEP07(2020)141
de Kerret H *et al* (Double Chooz) 2020 $\theta_{13}$ measurement via total neutron capture detection *Nat. Phys.* **16** 558–64
de Kerret H *et al* (Double Chooz) 2022 The double chooz antineutrino detectors arXiv:2201.13285
Declais Y *et al* 1994 Study of reactor anti-neutrino interaction with proton at bugey nuclear power plant *Phys. Lett.* B **338** 383–9
Declais Y *et al* 1995 Search for neutrino oscillations at 15-meters, 40-meters, and 95-meters from a nuclear power reactor at Bugey *Nucl. Phys.* B **434** 503–34
Deniz M *et al* (TEXONO) 2010 Measurement of Nu(e)-bar -electron scattering cross-section with a CsI (Tl) scintillating crystal array at the kuo-sheng nuclear power reactor *Phys. Rev.* D **81** 072001
Dent J B, Dutta B, Kim D, Liao S, Mahapatra R, Sinha K and Thompson A 2020 New directions for axion searches via scattering at reactor neutrino experiments *Phys. Rev. Lett.* **124** 211804
Dentler M, Esteban I, Kopp J and Machado P 2020 Decaying sterile neutrinos and the short baseline oscillation anomalies *Phys. Rev.* D **101** 115013
Dentler M, Hernández-Cabezudo Á, Kopp J, Maltoni M and Schwetz T 2017 Sterile neutrinos or flux uncertainties?—Status of the reactor anti-neutrino anomaly *J. High Energy Phys.* JHEP11(2017)099
Dentler M, Hernández-Cabezudo Á, Kopp J, Machado P A N, Maltoni M, Martinez-Soler I and Schwetz T 2018 Updated global analysis of neutrino oscillations in the presence of eV-scale sterile neutrinos *J. High Energy Phys.* JHEP08(2018)010
Denton P B 2022 Sterile neutrino search with MicroBooNE's electron neutrino disappearance data *Phys. Rev. Lett.* **129** 061801
Denton P B, Farzan Y and Shoemaker I M 2019 Activating the fourth neutrino of the 3+1 scheme *Phys. Rev.* D **99** 035003
Diaz A, Argüelles C A, Collin G H, Conrad J M and Shaevitz M H 2020 Where are we with light sterile neutrinos? *Phys. Rep.* **884** 1–59
Dutta D, Gandhi R, Kayser B, Masud M and Prakash S 2016 Capabilities of long-baseline experiments in the presence of a sterile neutrino *J. High Energy Phys.* JHEP11(2016)122
Dwyer D A and Langford T J 2015 Spectral structure of electron antineutrinos from nuclear reactors *Phys. Rev. Lett.* **114** 012502
Eguchi K *et al* (KamLAND) 2003 First results from KamLAND: evidence for reactor anti-neutrino disappearance *Phys. Rev. Lett.* **90** 021802
Ellis S A R, Kevin J K and Li S W 2020 Leptonic unitarity triangles *Phys. Rev.* D **102** 115027
Enqvist K K K and Thomson M J 1992 Stringent cosmological bounds on inert neutrino mixing *Nucl. Phys.* B **373** 498–528
Estienne M *et al* 2019 Updated summation model: an improved agreement with the daya bay antineutrino fluxes *Phys. Rev. Lett.* **123** 022502
Estrada J 2020 Observatory of skipper CCDs unveiling recoiling atoms https://astro.fnal.gov/science/dark-matter/oscura/
Fallot M *et al* 2012 New antineutrino energy spectra predictions from the summation of beta decay branches of the fission products *Phys. Rev. Lett.* **109** 202504
Fallot M, Littlejohn B R and Dimitriou P 2019 Antineutrino spectra and their applications *IAEA Report INDC(NDS)-0786* https://www-nds.iaea.org/publications/indc/indc-nds-0786.pdf
Feldman J and Cousins R 1998 *Phys. Rev.* D **57** 3873
Feng L, Zhang J-F and Zhang X 2017 A search for sterile neutrinos with the latest cosmological observations *Eur. Phys. J.* C **77** 418
Feng Peng A *et al* (Daya Bay) 2016c Measurement of the reactor antineutrino flux and spectrum at daya bay *Phys. Rev. Lett.* **116** 061801

Fernandez-Moroni G, Harnik R, Machado P A N, Martinez-Soler I, Perez-Gonzalez Y F, Rodrigues D and Rosauro-Alcaraz S 2021 The physics potential of a reactor neutrino experiment with skipper-ccds: searching for new physics with light mediators arXiv:2108.07310
Fijałkowska A *et al* 2017 *Phys. Rev. Lett.* **119** 052503
Fiorito L, Diez C J, Cabellos O, Stankovskiy A, Van den Eynde G and Labeau P E 2014 Fission yield covariance generation and uncertainty propagation through fission pulse decay heat calculation *Ann. Nucl. Energy* **69** 331–43
Flores L J *et al* (SBC, CE$\nu$NS Theory Group at IF-UNAM) 2021 Physics reach of a low threshold scintillating argon bubble chamber in coherent elastic neutrino-nucleus scattering reactor experiments *Phys. Rev.* D **103** L091301
Fomin A 2021 *Monte carlo simulation of neutrino-4 experiment, note Presented at Twentieth Lomonosov Conference* https://lomcon.ru/files/20LomCon/presentations/20Au_A/Fomin.pdf
Fong C, Sheng H, Minakata H and Nunokawa H 2017 A framework for testing leptonic unitarity by neutrino oscillation experiments *J. High Energy Phys.* JHEP02(2017)114
Formaggio J A and Zeller G P 2012 From eV to EeV: neutrino cross sections across energy scales *Rev. Mod. Phys.* **84** 1307–41
Fuss A *et al* 2022 EXCESS workshop: descriptions of rising low-energy spectra arXiv:2202.05097
Gandhi R, Kayser B, Masud M and Prakash S 2015 The impact of sterile neutrinos on CP measurements at long baselines *J. High Energy Phys.* JHEP11(2015)039
Gariazzo S, Giunti C and Laveder M 2013 Light sterile neutrinos in cosmology and short-baseline oscillation experiments *J. High Energy Phys.* JHEP11(2013)211
Gariazzo S, de Salas P F and Pastor S 2019 Thermalisation of sterile neutrinos in the early universe in the 3.1 scheme with full mixing matrix *J. Cosmol. Astropart. Phys.* JCAP07(2019)014
Gariazzo S, Giunti C, Laveder M and Li Y F 2017 Updated global 3.1 analysis of short-baseLine neutrino oscillations *J. High Energy Phys.* JHEP06(2017)135
Gariazzo S, Giunti C, Laveder M and Li Y F 2018 Model-independent $\bar{\nu}_e$ short-baseline oscillations from reactor spectral ratios *Phys. Lett.* B **782** 13–21
Ge S-F and Rodejohann W 2015 JUNO and neutrinoless double beta decay *Phys. Rev.* D **92** 093006
Gebre Y, Littlejohn B R and Surukuchi P T 2018 Prospects for improved understanding of isotopic reactor antineutrino fluxes *Phys. Rev.* D **97** 013003
Giunti C 2017a Improved determination of the $^{235}$U and $^{239}$Pu reactor antineutrino cross sections per fission *Phys. Rev.* D **96** 033005
Giunti C 2017b Precise determination of the $^{235}$U reactor antineutrino cross section per fission *Phys. Lett.* B **764** 145–9
Giunti C 2020 Statistical significance of reactor antineutrino active-sterile oscillations *Phys. Rev.* D **101** 095025
Giunti C and Laveder M 2010 Short-baseline $\bar{\nu}_\mu \to \bar{\nu}_e$ oscillations *Phys. Rev.* D **82** 093016
Giunti C and Laveder M 2011a 3+1 and 3+2 sterile neutrino fits *Phys. Rev.* D **84** 073008
Giunti C and Laveder M 2011b Statistical significance of the gallium anomaly *Phys. Rev.* C **83** 065504
Giunti C, Li Y F and Zhang Y Y 2020 KATRIN bound on 3.1 active-sterile neutrino mixing and the reactor antineutrino anomaly *J. High Energy Phys.* JHEP05(2020)061
Giunti C, Li Y F, Littlejohn B R and Surukuchi P T 2019 Diagnosing the reactor antineutrino anomaly with global antineutrino flux data *Phys. Rev.* D **99** 073005
Giunti C, Li Y F, Ternes C A and Zhang Y Y 2021 Neutrino-4 anomaly: oscillations or fluctuations? *Phys. Lett.* B **816** 136214
Giunti C, Li Y F, Ternes C A and Xin Z 2022 Reactor antineutrino anomaly in light of recent flux model refinements *Phys. Lett.* B **829** 137054
Giunti C, Ji X P, Laveder M, Li Y F and Littlejohn B R 2017 Reactor fuel fraction information on the antineutrino anomaly *J. High Energy Phys.* JHEP10(2017)143
Goldhagen K, Maltoni M, Reichard S E and Schwetz T 2022 Testing sterile neutrino mixing with present and future solar neutrino data *Eur. Phys. J.* C **82** 116
Greenwood Z D *et al* 1996 Results of a two position reactor neutrino oscillation experiment *Phys. Rev.* D **53** 6054–64
Greenwood R C, Helmer R G, Putnam M H and Watts K D 1997 Measurement of beta-decay intensity distributions of several fission-product isotopes using a total absorption gamma-ray spectrometer *Nucl. Inst. Meth.* A **390** 95–154
Guadilla V *et al* 2019a Large impact of the decay of niobium isomers on the reactor $\bar{\nu}_e$ summation calculations *Phys. Rev. Lett.* **122** 042502

Guadilla V *et al* 2019b Total absorption $\gamma$-ray spectroscopy of niobium isomers *Phys. Rev.* C **100** 024311
Guadilla V *et al* 2019c Total absorption $\gamma$-ray spectroscopy of the $\beta$-delayed neutron emitters $^{137}$I and $^{95}$Rb *Phys. Rev.* C **100** 044305
Guillermo Fernández M 2021 Installing a Skipper-CCD sensor in Atucha 2 power reactor: current status, note Presented at Magnificent CE$\nu$NS 2021
Haghighat A, Huber P, Li S, Link J M, Mariani C, Park J and Subedi T 2020 Observation of reactor antineutrinos with a rapidly-deployable surface-level detector *Phys. Rev. Appl.* **13** 034028
Hagstotz S, Pablo F d S, Gariazzo S, Gerbino M, Lattanzi M, Vagnozzi S, Freese K and Pastor S 2021 Bounds on light sterile neutrino mass and mixing from cosmology and laboratory searches *Phys. Rev.* D **104** 123524
Hahn A A *et al* 1989 Anti-neutrino spectra From $^{241}$Pu and $^{239}$Pu thermal neutron fission products *Phys. Lett.* **B218** 365–8
Hahn A A, Schreckenbach K, Gelletly W, von Feilitzsch F, Colvin G and Krusche B 1989 Antineutrino spectra from 241pu and 239pu thermal neutron fission products *Phys. Lett.* B **218** 365–8
Hampel W *et al* (GALLEX) 1998 Final results of the $^{51}$Cr neutrino source experiments in GALLEX *Phys. Lett.* B **420** 114–26
Hannestad S, Tamborra I and Tram T 2012 Thermalisation of light sterile neutrinos in the early universe *J. Cosmol. Astropart. Phys.* JCAP07(2012)025
Harrison P F, Perkins D H and Scott W G 2002 Tri-bimaximal mixing and the neutrino oscillation data *Phys. Lett.* B **530** 167
Hayen L, Kostensalo J, Severijns N and Suhonen J 2019 First-forbidden transitions in the reactor anomaly *Phys. Rev.* C **100** 054323
Hayes A C and Vogel P 2016 Reactor neutrino spectra *Ann. Rev. Nucl. Part. Sci.* **66** 219–44
Hayes A C, Friar J L, Garvey G T, Jungman G and Jonkmans G 2014 Systematic uncertainties in the analysis of the reactor neutrino anomaly *Phys. Rev. Lett.* **112** 202501
Hayes A C, Jungman G, McCutchan E A, Sonzogni A A, Garvey G T and Wang X 2018 Analysis of the daya bay reactor antineutrino flux changes with fuel burnup *Phys. Rev. Lett.* **120** 022503
Hayes A C, Friar J L, Garvey G T, Ibeling D, Jungman G, Kawano T and Mills R W 2015 Possible origins and implications of the shoulder in reactor neutrino spectra *Phys. Rev.* D **92** 033015
He X and Gang A 2003 Some simple mixing and mass matrices for neutrinos *Phys. Lett.* B **560** 87–90
Helena A M *et al* (STEREO) 2021 First antineutrino energy spectrum from $^{235}$U fissions with the STEREO detector at ILL *J. Phys.*G **48** 075107
Hill R J and Mikhail P S 2015 Standard Model anatomy of WIMP dark matter direct detection: II. QCD analysis and hadronic matrix elements *Phys. Rev.* D **91** 043505
Hoummada A, Lazrak Mikou S, Avenier M, Bagieu G, Cavaignac J F and Holm Koang D 1995 Neutrino oscillations I.L.L. experiment reanalysis *Appl. Radiat. Isot.* **46** 449
Huber P 2011 On the determination of anti-neutrino spectra from nuclear reactors *Phys. Rev.* C **84** 024617
Jaffke P and Huber P 2017 Determining reactor fuel type from continuous antineutrino monitoring *Phys. Rev. Appl.* **8** 034005
Javier T, Sofo-Haro M, Drlica-Wagner A, Essig R, Guardincerri Y, Holland S, Volansky T and Yu T-T 2017a Single-electron and single-photon sensitivity with a silicon skipper CCD *Phys. Rev. Lett.* **119** 131802
Javier T, Sofo-Haro M, Drlica-Wagner A, Essig R, Guardincerri Y, Holland S, Volansky T and Yu T-T 2017b Single-electron and single-photon sensitivity with a silicon skipper CCD *Phys. Rev. Lett.* **119** 131802
Jones K W and Kraner H W 1975 Energy lost to ionization by 254-ev $^{73}$Ge atoms stopping in Ge *Phys. Rev.* A **11** 1347–53
Kaether F, Hampel W, Heusser G, Kiko J and Kirsten T 2010 Reanalysis of the GALLEX solar neutrino flux and source experiments *Phys. Lett.* B **685** 47–54
Kerman S, Sharma V, Deniz M, Wong H T, Chen J W, Li H B, Lin S T, Liu C P, Yue Q *et al* (TEXONO) 2016 Coherency in neutrino-nucleus elastic scattering *Phys. Rev.* D **93** 113006
Kim B R *et al* 2015 Pulse shape discrimination capability of metal-loaded organic liquid scintillators for a short-baseline reactor neutrino experiment *Phys. Scr.* **90** 055302
Klop N and Palazzo A 2015 Imprints of CP violation induced by sterile neutrinos in T2K data *Phys. Rev.* D **91** 073017

Knee A M, Contreras D and Scott D 2019 Cosmological constraints on sterile neutrino oscillations from planck *J. Cosmol. Astropart. Phys.* JCAP07(2019)039
Ko Y J 2016 *Status of NEOS-II, Neutrino 2020: 29th Int. Conf. on Neutrino Physics and Astrophysics*
Ko Y J *et al* (NEOS) 2017 Sterile neutrino search at the NEOS experiment *Phys. Rev. Lett.* **118** 121802
Kopeikin V I, Yu N P and Sabelnikov A A 2021 Measurement of the ratio of cumulative spectra of beta particles from $^{235}$U and $^{239}$Pu fission products for solving problems of reactor-antineutrino physics *Phys. Atom. Nucl.* **84** 1–10
Kopeikin V, Skorokhvatov M and Titov O 2021 Reevaluating reactor antineutrino spectra with new measurements of the ratio between $^{235}$U and $^{239}$Pu $\beta$ spectra *Phys. Rev.* D **104** L071301
Kopp J, Maltoni M and Schwetz T 2011 Are there sterile neutrinos at the eV scale? *Phys. Rev. Lett.* **107** 091801
Kopp J, Pedro A N M, Maltoni M and Schwetz T 2013 Sterile neutrino oscillations: the global picture *J. High Energy Phys.* JHEP05(2013)050
Kwon H *et al* 1981 Search for neutrino oscillations at a fission reactor *Phys. Rev.* D **24** 1097–111
Lenardo B G *et al* 2019 Low-energy physics reach of xenon detectors for nuclear-recoil-based dark matter and neutrino experiments *Phys. Rev. Lett.* **123** 231106
Li V A, Timothy M C, Dazeley S A, Duvall M J, Jovanovic I, Mabe A N, Reedy E T E and Sutanto F 2019 A prototype for sandd: A highly-segmented pulse-shape-sensitive plastic scintillator detector incorporating silicon photomultiplier arrays *Nucl. Inst. Meth.* A **942** 162334
Liao J, Marfatia D and Whisnant K 2019 MiniBooNE, MINOS+ and IceCube data imply a baroque neutrino sector *Phys. Rev.* D **99** 015016
Littlejohn B, Luk K B and Ochoa-Ricoux J P 2020 Legacy of the daya bay reactor neutrino experiment *Snowmass 2021 Letter of Interest*
Maltoni M and Schwetz T 2007 Sterile neutrino oscillations after first MiniBooNE results *Phys. Rev.* D **76** 093005
Manfred L, Merle A and Rodejohann W 2006 Improved limit on $\theta_{13}$ and implications for neutrino masses in neutrino-less double beta decay and cosmology *Phys. Rev.* D **73** 053005
Matthews E F, Lee A B and Younes W 2021 Stochastically estimated covariance matrices for independent and cumulative fission yields in the ENDF/B-VIII.0 and JEFF-3.3 evaluations *At. Data Nucl. Data Tables* **140** 101441
Melchiorri A, Mena O, Palomares-Ruiz S, Pascoli S, Slosar A and Sorel M 2009 Sterile neutrinos in light of recent cosmological and oscillation data: a multi-flavor scheme approach *J. Cosmol. Astropart. Phys.* JCAP01(2009)036
Mention G, Fechner M, Lasserre T, Mueller T, Lhuillier D, Cribier M and Letourneau A 2011 The reactor antineutrino anomaly *Phys. Rev.* D **83** 073006
Mirizzi A, Mangano G, Saviano N, Borriello E, Giunti C, Miele G and Pisanti O 2013 The strongest bounds on active-sterile neutrino mixing after Planck data *Phys. Lett.* B **726** 8–14
Moss Z, Marjon H M, Argüelles C A and Conrad J M 2018 Exploring a nonminimal sterile neutrino model involving decay at IceCube *Phys. Rev.* D **97** 055017
Mueller T A *et al* 2011 Improved predictions of reactor antineutrino spectra *Phys. Rev.* C **83** 054615
Nasteva I *et al* (CONNIE) 2021 Low-energy reactor neutrino physics with the CONNIE experiment arXiv:2110.13620
Ni K 2020 Feasibility of a Liquid Xenon Detector for Reactor Neutrino Detection via CE$\nu$NS, note Presented at Magnificent CE$\nu$NS
Ni K, Qi J, Shockley E and Wei Y 2021 Sensitivity of a liquid xenon detector to neutrino–nucleus coherent scattering and neutrino magnetic moment from reactor neutrinos *Universe* **7** 54
Ochoa-Ricoux J P, Wang W, Wen L and Wurm M 2020 The JUNO experiment *Snowmass 2021 Letter of Interest*
Pasierb E, Gurr H S, Lathrop J, Reines F and Sobel H W 1979 Detection of weak neutral current using fission $\bar{\nu}_e$ on deuterons *Phys. Rev. Lett.* **43** 96
Plompen A J M *et al* 2020 The joint evaluated fission and fusion nuclear data library, JEFF-3.3 *Eur. Phys. J.* A **56** 181
PROSPECT Collaboration 2020a The expanded physics reach of PROSPECT-II *Snowmass 2021 Letter of Interest*
PROSPECT Collaboration 2020c PROSPECT: a case study of neutrino physics research providing enabling capabilities for nuclear security applications *Snowmass 2021 Letter of Interest*
Qian X and Peng J-C 2019 Physics with reactor neutrinos *Rep. Prog. Phys.* **82** 036201

Qian X, Zhang C, Diwan M and Vogel P 2013 Unitarity tests of the neutrino mixing matrix arXiv:1308.5700
Rasco B C *et al* 2016 Decays of the three top contributors to the reactor $\overline{\nu}_e$ high-energy spectrum, $^{92}$Rb , $^{96}gs$Y, and $^{142}$Cs, studied with total absorption spectroscopy *Phys. Rev. Lett.* **117** 092501
Reines F and Cowan C L 1959 Free anti-neutrino absorption cross-section: I. Measurement of the free anti-neutrino absorption cross-section by protons *Phys. Rev.* **113** 273–9
Reines F, Gurr H S and Sobel H W 1976 Detection of anti-electron-neutrino e scattering *Phys. Rev. Lett.* **37** 315–8
Rice S *et al* 2017 Total absorption spectroscopy study of the $\beta$ decay of $^{86}$Br and $^{91}$Rb *Phys. Rev.* C **96** 014320
Ritz S *et al* (HEPAP Subcommittee) 2014 for discovery: strategic plan for U.S. Particle physics in the global context https://www.usparticlephysics.org/wp-content/uploads/2018/03/FINAL_P5_Report_053014.pdfBuilding
ROADSTR Near-Field Working Group 2020 ROADSTR: a mobile antineutrino detector platform for enabling multi-reactor spectrum, oscillation, and application measurements *Snowmass 2021 Letter of Interest*
Romano C *et al* 2022 *Nuclear Data to Reduce Uncertainties in Reactor Antineutrino Measurements: Summary Report of the Workshop on Nuclear Data for Reactor Antineutrino Measurements (WoNDRAM)* https://www.osti.gov/servlets/purl/1842423/
Runkle R C, Bernstein A and Vanier P E 2010 Securing special nuclear material: Recent advances in neutron detection and their role in nonproliferation *J. Appl. Phys.* **108** 111101
Schael S *et al* (ALEPH, DELPHI, L3, OPAL, SLD, LEP Electroweak Working Group, SLD Electroweak Group, SLD Heavy Flavour Group) 2006 Precision electroweak measurements on the *Z resonance Phys. Rep.* **427** 257–454
Scholz B J, Chavarria A E, Collar J I, Privitera P and Robinson A E 2016 Measurement of the low-energy quenching factor in germanium using an $^{88}$Y/Be photoneutron source *Phys. Rev.* D **94** 122003
Schoppmann S 2023 Review of novel approaches to organic liquid scintillators in neutrino physics *Symmetry* **15** 11
Schreckenbach K, Colvin G, Gelletly W and Von Feilitzsch F 1985 Determination of the antineutrino spectrum from 235u thermal neutron fission products up to 9.5 mev *Phys. Lett.* B **160** 325–30
Serebrov A P *et al* (NEUTRINO-4) 2019 First observation of the oscillation effect in the neutrino-4 experiment on the search for the sterile neutrino *Pisma Zh. Eksp. Teor. Fiz.* **109** 209–18
Serebrov A *et al* (Neutrino-4) 2021 Search for sterile neutrinos with the neutrino-4 experiment and measurement results *Phys. Rev.* D **104** 032003
Settimo M 2020 Search for low-mass dark matter with the DAMIC experiment arXiv:2003.09497
Sharma V *et al* (TEXONO) 2021 Studies of quantum-mechanical coherency effects in neutrino-nucleus elastic scattering *Phys. Rev.* D **103** 092002
Singh L *et al* (TEXONO) 2019 Constraints on millicharged particles with low threshold germanium detectors at kuo-sheng reactor neutrino laboratory *Phys. Rev.* D **99** 032009
Soma A K *et al* (TEXONO) 2016 Characterization and performance of germanium detectors with sub-keV sensitivities for neutrino and dark matter experiments *Nucl. Instrum. Meth.* A **836** 67–82
Sonzogni A A, Johnson T D and McCutchan E A 2015 Nuclear structure insights into reactor antineutrino spectra *Phys. Rev.* C **91** 011301
Sonzogni A A, McCutchan E A and Hayes A C 2017 Dissecting reactor antineutrino flux calculations *Phys. Rev. Lett.* **119** 112501
Sonzogni A A, Lorek R J, Mattera A and McCutchan E A 2022 Can decay heat measurements tell us something about the reactor antineutrino anomaly? arXiv:2203.02382
Strauss R *et al* 2017 The $\nu$-cleus experiment: a gram-scale fiducial-volume cryogenic detector for the first detection of coherent neutrino-nucleus scattering *Eur. Phys. J.* C **77** 506
Tuli J K 1996 *Nucl. Inst. Meth.* A **369** 506
Valencia E *et al* 2017 Total absorption $\gamma$-ray spectroscopy of $\beta$-delayed neutron emitters $^{87}$Br, $^{88}$Br and $^{94}$Rb *Phys. Rev.* C **95** 024320
Vidal M 2020 *NEWS-G: Status, Presented at Magnificent CEνNS 2020*
Vinyoles N, Serenelli A M, Villante F L, Basu S, Bergström J, Gonzalez-Garcia M C, Maltoni M, Peña Garay C and Song N 2017 A new generation of standard solar models *Astrophys. J.* **835** 202
Vogel P and Beacom J F 1999 Angular distribution of neutron inverse beta decay *Phys. Rev.* D **60** 053003

Vogel P, Wen L and Zhang C 2015 Neutrino oscillation studies with reactors *Nat. Commun.* **6** 6935
Vogel P, Schenter G K, Mann F M and Schenter R E 1981 Reactor anti-neutrino spectra and their application to anti-neutrino induced reactions. 2 *Phys. Rev.* C **24** 1543–53
von Feilitzsch F, Hahn A A and Schreckenbach K 1982 Experimental beta-spectra from $^{239}$Pu and $^{235}$U thermal neutron fission products and their correlated antineutrino spectra *Phys. Lett.* B **118** 162–6
Von Feilitzsch F, Hahn A A and Schreckenbach K 1982 Experimental beta-spectra from Pu-239 and U-235 thermal neutron fission products and their correlated antineutrino spectra *Phys. Lett.* **B118** 162–6
Wagner S, Grassi M and Cabrera A 2018 A hybrid organic/inorgaic scintillator for high performance measurements arXiv:1807.00628
Wang J *et al* (JUNO) 2022 Damping signatures at JUNO, a medium-baseline reactor neutrino oscillation experiment *J. High Energy Phys.* JHEP06(2022)062
Wang X B, Friar J L and Hayes A C 2016 Nuclear zemach moments and finite-size corrections to allowed $\beta$ decay *Phys. Rev.* C **94** 034314
Way K and Wigner E 1948 *Phys. Rev.* **73** 1318
Workshop, EXCESS (2021), https://indico.cern.ch/event/1013203/ EXCESS Workshop 2021
Workman R L *et al* (Particle Data Group) 2022 Review of particle physics *PTEP* **2022** 083C01
Xing Z-z 2002 Nearly tri bimaximal neutrino mixing and CP violation *Phys. Lett.* B **533** 85–93
Xu J 2021 *Status of the CHILLAX Detector Development, Presented at Magnificent CEνNS 2021*
Yeh M *et al* 2011 A new water-based liquid scintillator and potential applications *Nucl. Instrum. Meth.* A **660** 51–6
Zaitseva N, Glenn A, Paul Martinez H, Carman L, Pawełczak I, Faust M and Payne S 2013 Pulse shape discrimination with lithium-containing organic scintillators *Nucl. Inst. Meth.* A **729** 747–54
Zaitseva N, Rupert B L, PaweŁczak I, Glenn A, Martinez H P, Carman L, Faust M, Cherepy N and Payne S 2012 Plastic scintillators with efficient neutron/gamma pulse shape discrimination *Nucl. Inst. Meth.* A **668** 88–93
Zakari-Issoufou A A *et al* (IGISOL) 2015 Total absorption spectroscopy study of $^{92}$Rb decay: a major contributor to reactor antineutrino spectrum shape *Phys. Rev. Lett.* **115** 102503
Zhang C, Qian X and Vogel P 2013 Reactor antineutrino anomaly with known $\theta_{13}$ *Phys. Rev.* D **87** 073018
Zyla P A *et al* (Particle Data Group) 2020 Review of particle physics *PTEP* **2020** 083C01